Geological Society of America
Memoir 194
2001

Uplift, exhumation, and deformation in the Chinese Tian Shan

Trevor A. Dumitru, Da Zhou*, Edmund Z. Chang, and Stephan A. Graham
Department of Geological and Environmental Sciences, Stanford University, Stanford, California 94305, USA
Marc S. Hendrix
Department of Geology, University of Montana, Missoula, Montana 59812, USA
Edward R. Sobel
Institut für Geowissenschaften, Universität Potsdam, D-14415 Potsdam, Germany
Alan R. Carroll
Department of Geology and Geophysics, University of Wisconsin, Madison, Wisconsin 53706, USA

ABSTRACT

The terranes composing the basement of the Tian Shan were originally sutured together during two collisions in Late Devonian–Early Carboniferous and Late Carboniferous–Early Permian time. Since then, the range has repeatedly been uplifted and structurally reactivated, apparently as a result of the collision of island arcs and continental blocks with the southern margin of Asia far to the south of the range. Evidence for these deformational episodes is recorded in the sedimentary histories of the Junggar and Tarim foreland basins to the north and south of the range and by the cooling and exhumation histories of rocks in the interior of the range. Reconnaissance apatite fission-track cooling ages from the Chinese part of the range cluster in three general time periods, latest Paleozoic, late Mesozoic, and late Cenozoic. Latest Paleozoic cooling is recorded at Aksu (east of Kalpin) on the southern flank of the range, at two areas in the central Tian Shan block along the Dushanzi-Kuqa Highway, and by detrital apatites at Kuqa that retain fission-track ages of their sediment source areas. Available $^{40}Ar/^{39}Ar$ cooling ages from the range also cluster within this time interval, with very few younger ages. These cooling ages may record exhumation and deformation caused by the second basement suturing collision between the Tarim–central Tian Shan composite block and the north Tian Shan.

Apatite data from three areas record late Mesozoic cooling, at Kuqa on the southern flank of the range and at two areas in the central Tian Shan block. Sedimentary sections in the Junggar and Tarim foreland basins contain major unconformities, thick intervals of alluvial conglomerate, and increased subsidence rates between about 140 and 100 Ma. These data may reflect deformation and uplift induced by collision of the Lhasa block with the southern margin of Asia in latest Jurassic–Early Cretaceous time. Large Jurassic intermontane basins are preserved within the interior of the Tian Shan and in conjunction with the fission-track data suggest that the late Mesozoic Tian Shan was subdivided into a complex of generally east-west–trending, structurally controlled subranges and basins.

Apatite data from five areas record major late Cenozoic cooling, at sites in the basin-vergent thrust belts on the northern and southern margins of the range, and along the north Tian Shan fault system in the interior of the range. The thrust belts

*Now at ExxonMobile Exploration Company, P.O. Box 4778, Houston, Texas 77060, USA

Dumitru, T.A., et al., 2001, Uplift, exhumation, and deformation in the Chinese Tian Shan, *in* Hendrix, M.S., and Davis, G.A., eds., Paleozoic and Mesozoic tectonic evolution of central Asia: From continental assembly to intracontinental deformation: Boulder, Colorado, Geological Society of America Memoir 194, p. 71–99.

and fault system have been sites of active shortening and exhumation since at least ca. 25 Ma, apparently induced by the collision of the Indian subcontinent with the southern margin of Asia. On the basis of regional relations, the north Tian Shan fault system is likely an important active right-lateral transpressional structure that has reactivated the north Tian Shan–central Tian Shan suture zone.

In general, most of the Chinese Tian Shan appears to have been exhumed only limited amounts through Mesozoic and Cenozoic time. Within our sampling areas, only limited areas along the north Tian Shan fault zone and in parts of the range-margin thrust belts were exhumed more than ~3 km during the Cenozoic India-Asia collision. Modern intermontane basins are present within the Tian Shan and help divide it into a number of subranges, much like the late Mesozoic Tian Shan. This modern physiography likely reflects in part reactivation of pre-Cenozoic structural trends.

INTRODUCTION

The Tian Shan (Heavenly Mountains) extends east-west for ~2500 km through western China, Kazakstan, and Kirghizstan and reaches elevations as high as 7400 m (Figs. 1 and 2). Much of the modern relief of the range is a result of contraction and uplift driven by the collision of the India subcontinent with the southern margin of Asia, which began in early Tertiary time and continues today (e.g., Patriat and Achache, 1984; Tapponnier et al., 1986; Klootwijk et al., 1992; Avouac et al., 1993; Sobel and Dumitru, 1997). However, the basement terranes composing the Tian Shan were originally sutured together by Late Carboniferous–Early Permian time (e.g., Allen et al., 1992; Carroll et al., 1995; Zhou et al., this volume) and since then have been subjected to repeated structural reactivations. These reactivations may have been caused by earlier collisions of smaller continental fragments and volcanic arcs with the southern margin of Asia, such as the collision of the Qiangtang block in Late Triassic time and the Lhasa block in latest Jurassic–Early Cretaceous time (Fig. 1) (e.g., Hendrix et al., 1992).

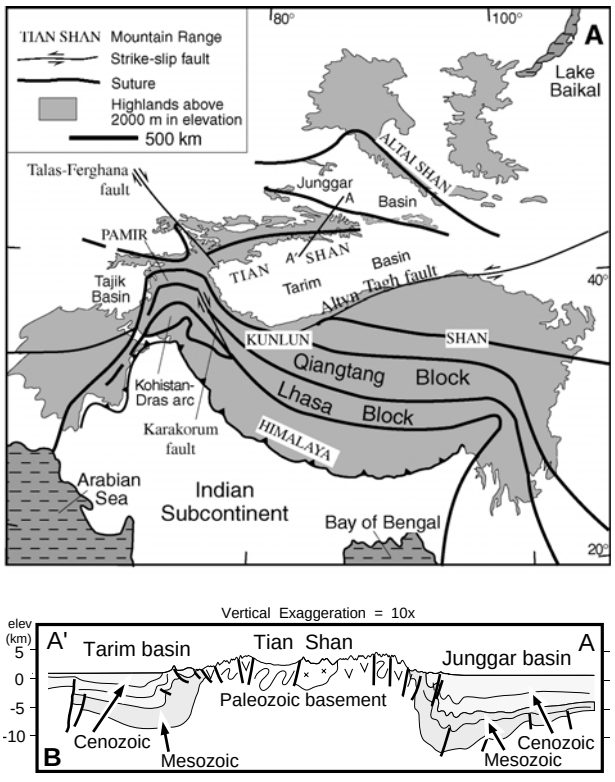

Figure 1. A: Schematic map of central Asia showing location of Tian Shan within context of basins and highlands formed by Cenozoic collision between India and southern margin of Asia. Also shown are Qiangtang block, Lhasa block, and Kohistan-Dras arc, which collided with southern margin of Asia in Mesozoic time. Modified from Watson et al. (1987). B: Cross section showing deformed Paleozoic and older basement in core of Tian Shan and Mesozoic-Cenozoic foreland basins on flanks of range. Foreland basin strata have been thrust outward from range core during Cenozoic shortening driven by India-Asia collision.

Very little is known about the postassembly deformational history of the Tian Shan, particularly in pre-Cenozoic time. In conjunction with stratigraphic and sedimentological studies in the Chinese part of the range, we have collected about 65 rock samples for apatite fission-track analysis. The apatite fission-track method may be used to date the cooling of rock units through the subsurface temperature window of about 125 °C to 60 °C. Assuming a nominal geothermal gradient of about 22 °C/km (discussed further in the following), this is equivalent to exhumation up through a depth window of about 5–2 km beneath the Earth's surface. Such cooling is commonly a result of uplift and exhumation of rock units during large-scale deformation in the upper crust and so may be used to constrain the timing, magnitude, and location of such deformation.

The 65 fission-track samples make an extremely sparse sampling set for a mountain range as large and complex as the Tian Shan, so results of this study are necessarily reconnaissance in nature. Different areas of the range retain fission-track records of a variety of cooling events ranging in age from late Paleozoic to late Cenozoic. The available data show a tendency for these events to cluster in three general time periods, referred to here as the latest Paleozoic, late Mesozoic, and late Cenozoic cooling episodes, which appear to correlate in time with significant plate margin collisional events.

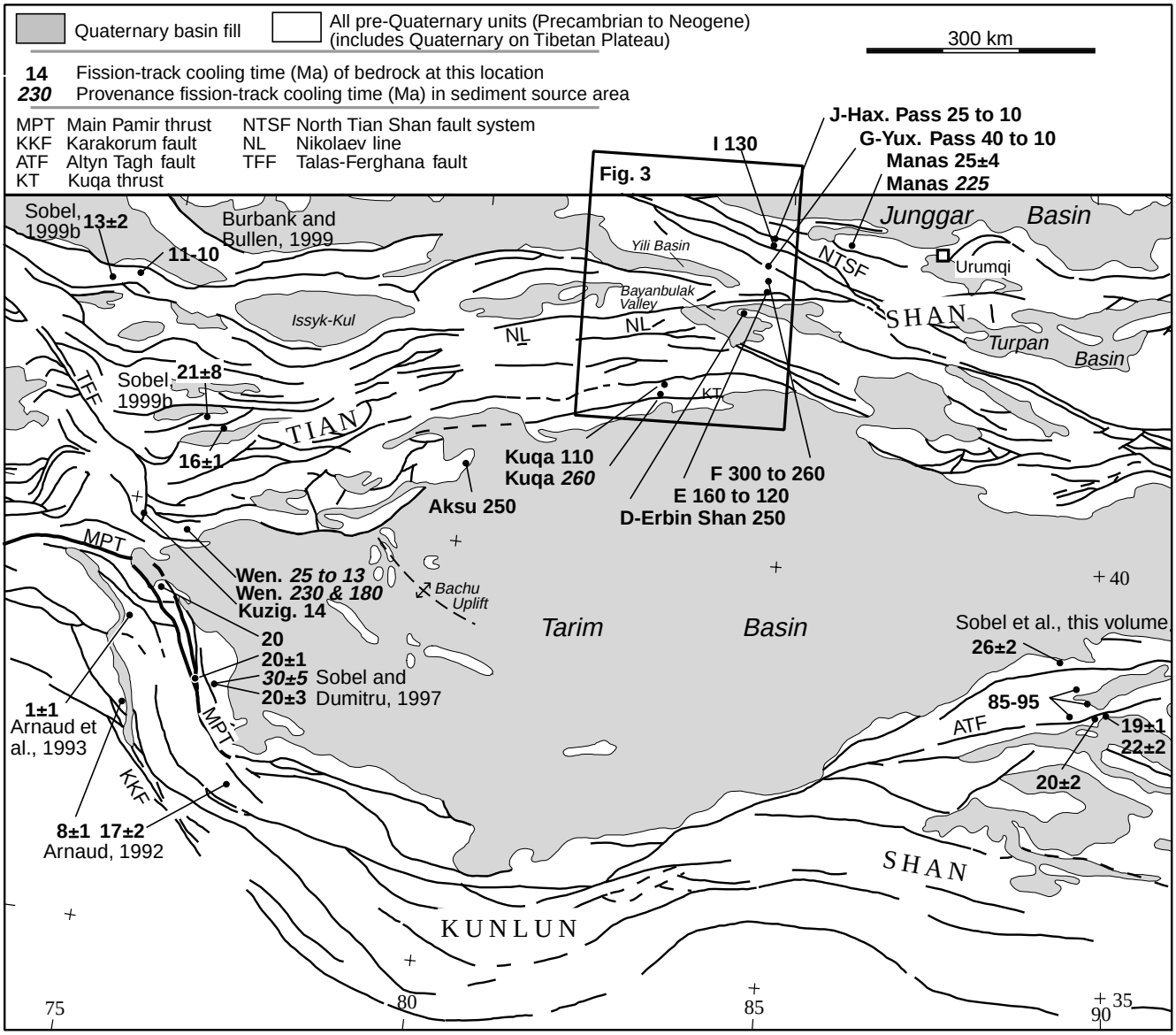

Figure 2. Map of Tian Shan, Tarim basin, and surrounding areas summarizing main structures and predominate times of cooling below 100 °C derived from fission-track data. Map modified from Academy of Geological Sciences of China (1975), Xinjiang Bureau of Geology and Mineral Resources (1985), Chen et al. (1985), Jiao et al. (1988), Pan (1992), and Brunel et al. (1994).

BACKGROUND GEOLOGY AND TECTONIC HISTORY

The basement terranes currently exposed in the Tian Shan amalgamated during two poorly understood Paleozoic collisional events, a Late Devonian to Early Carboniferous collision between the Tarim and central Tian Shan blocks, followed by a Late Carboniferous–Early Permian collision between the Tarim–central Tian Shan composite block and island arcs currently exposed in the north Tian Shan and Bogda Shan (e.g., Fig. 3) (Wang et al., 1990; Allen et al., 1992; Carroll et al., 1995, this volume; Zhou et al., this volume). Widespread Carboniferous granitic intrusions and Early Permian rhyolitic and basaltic eruptions represent the last significant igneous activity in the range (Allen et al., 1992; Carroll et al., 1995, this volume).

Landsat imagery, Chinese regional maps, seismicity, and local field studies suggest that latest Cenozoic strain in the Chinese part of the range is concentrated in basin-vergent thrust systems on the northern and southern margins of the range (Fig. 3) (e.g., Tapponnier and Molnar, 1979; Xinjiang Bureau of Geology and Mineral Resources [BGMR], 1985, 1993; Ma, 1986; Avouac et al., 1993; Roecker et al., 1993; Yin et al., 1998). Very few data have been published about the structural history of the interior of the range. Tapponnier and Molnar (1979) used Landsat imagery to identify a network of very large active east-northeast– and west-northwest–striking strike-slip fault systems

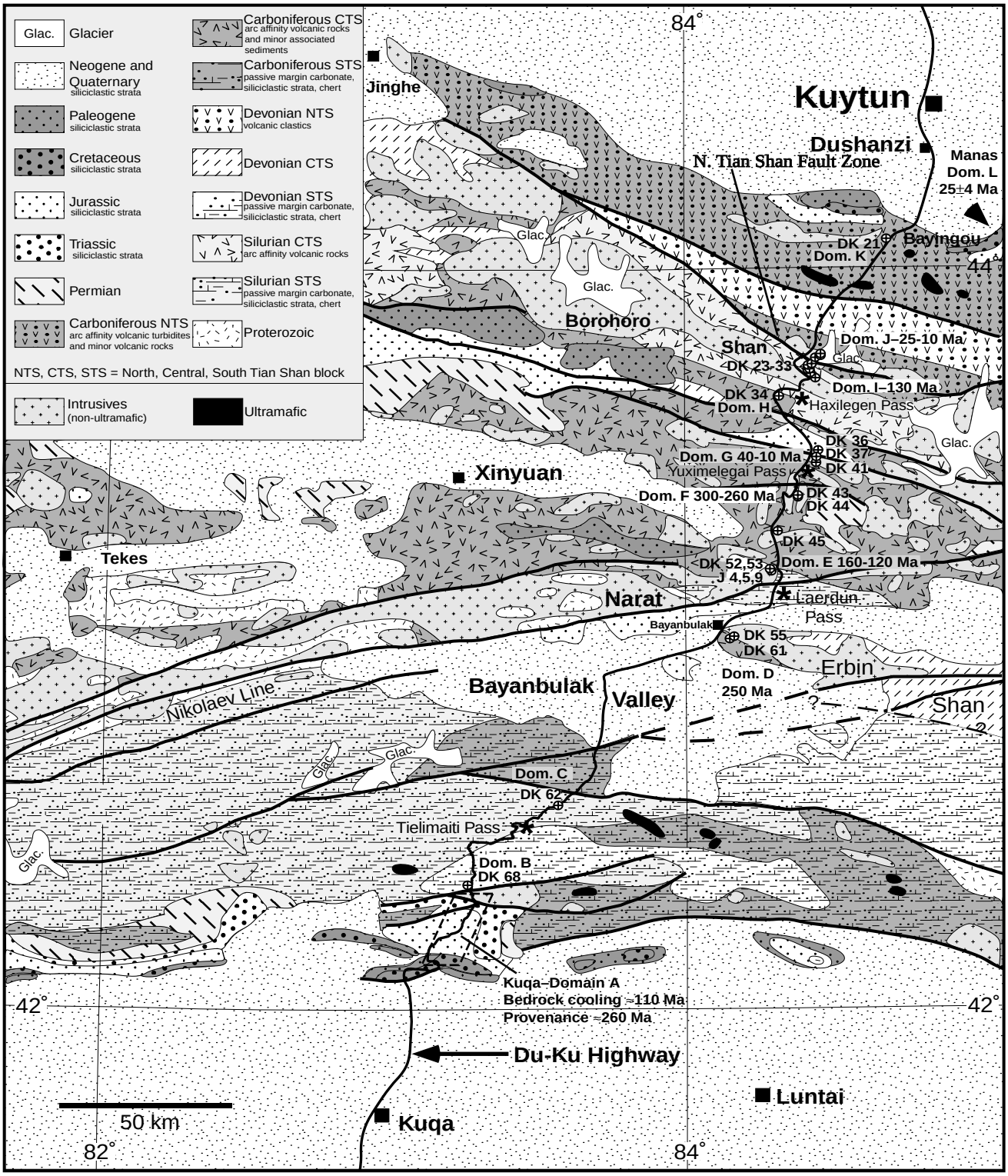

Figure 3. Geologic map of Dushanzi-Kuqa Highway corridor across Tian Shan, and fission-track data. Range is composed of three strongly deformed Paleozoic assemblages: (1) south Tian Shan, characterized by passive margin succession overlying Tarim block basement; (2) central Tian Shan block characterized by abundant arc affinity volcanic rocks; and (3) north Tian Shan, also characterized by abundant arc affinity volcanic rocks. Weakly deformed Jurassic strata in interior of range are remnants of Mesozoic intermontane basins. East-west–trending belts of Mesozoic and Cenozoic siliciclastic strata on northern and southern margins of range mark locations of Cenozoic basin-vergent thrust belts. North Tian Shan fault zone appears to be Cenozoic strike-slip or transpressional structure that has reactivated Paleozoic suture between central Tian Shan and north Tian Shan. Map from Zhou et al. (this volume), based on proprietary mapping by Xinjiang Bureau of Geology and Mineral Resources. Note that many contacts on map are faults; only most important faults are shown. Fission-track sample locations and data domains (A–L) are indicated. Ages indicated for most domains are main times of bedrock cooling below ~100 °C indicated by fission-track modeling.

in central Asia, which they inferred to have accommodated eastward lateral escape of crustal blocks induced by the collision of India with Asia. One such structure, the Talas-Ferghana fault, cuts across the Tian Shan in Kazakstan and Kirghizstan (Figs. 1 and 2) (e.g., Burtman et al., 1996; Sobel, 1999a). Many recent compilation maps show a major active west-northwest–striking, right-lateral, strike-slip or transpressional structure, sometimes named the north Tian Shan fault system, crossing the core of the range in China (Figs. 2 and 3) (e.g., Xinjiang BGMR, 1985, 1993; Ma, 1986; Hendrix et al., 1992; Yin et al., 1998; Zhou et al., this volume). However, this structure was not identified by Tapponnier and Molnar (1979), and data documenting Cenozoic offset along it do not appear to have been published. Almost all published K-Ar and $^{40}Ar/^{39}Ar$ ages from the Tian Shan are older than about 250 Ma (Yin et al., 1998; Zhou et al., this volume), suggesting that all metamorphism and ductile fabrics in the sampled areas are Paleozoic or older, and that post-Paleozoic exhumation has totaled $<\sim$15 km.

Substantial work has been done on the sedimentological and structural histories of the Paleozoic to Holocene Tarim and Junggar basins, which flank the Tian Shan on the south and north (Figs. 1–3) (Hendrix et al., 1992; Carroll et al., 1995, this volume; Li et al., 1996; Sobel and Dumitru, 1997; Yin et al., 1998; Sobel, 1999a). These basins resided in foreland settings during Mesozoic and Cenozoic time, and the basin margins have been uplifted and exhumed by late Cenozoic folding and thrusting and thus are exposed for study (e.g., Figs. 1B and 3). This folding and thrusting generally verges out from the range and into the basins and presumably reflects compressive stresses transmitted to the Tian Shan from the India-Asia collision zone far to the south. In this chapter we refer to these exposed sedimentary rocks as the Tarim and Junggar thrust belts and use the term Tian Shan core for the rocks exposed in the interior of the range. Paleocurrent and provenance data from the two thrust belts indicate that the core of the Tian Shan generally formed a persistent topographic high from late Paleozoic to Holocene time, shedding detritus into the basins to the north and south (Carroll et al., 1990, 1995, this volume; Hendrix et al., 1992; Graham et al., 1993; Hendrix, 2000). Geographically widespread episodes of particularly coarse grained sedimentation and erosional unconformities within the basin sections record renewed deformation in the core of the range at several times, suggesting that Mesozoic accretion of smaller terranes onto the south Asian continental margin uplifted the Tian Shan, presumably by reactivating Carboniferous–Permian structures, analogous to the major deformation induced by the Cenozoic collision of the Indian subcontinent (Hendrix et al., 1992). However, there is as yet essentially no direct evidence of deformation within the core of the range. In particular, slip during the Mesozoic does not appear to have been definitively documented on any faults within the Chinese part of the Tian Shan.

The Cenozoic strata exposed in the foreland thrust belts potentially retain important information on the deformation and uplift of the Tian Shan during the India-Asia collision. However, control on the depositional ages of these clastic strata has generally proven problematic. Sobel and Dumitru (1997) concluded that published data on Cenozoic sediments exposed around the western Tarim basin did not reliably constrain the timing of initiation of Cenozoic deformation in the Tian Shan. Yin et al. (1998) suggested that initial significant thrusting in the northern Tarim basin at Kuqa (Figs. 2 and 3) may have begun at 24–21 Ma, based on a tentative magnetostratigraphic age assignment for a facies change from lacustrine to braided-fluvial deposition.

There are several especially noteworthy aspects of Cenozoic deformation in the Tian Shan. First, the Tian Shan lies more than 1000 km north of the Indus-Tsangpo suture, which marks the collision between India and Asia (Fig. 1). Thus, stresses from the collision have been transmitted remarkably long distances to deform the Tian Shan, while the intervening Tarim basin has remained relatively undeformed (e.g., Li et al., 1996). Second, the India-Asia collision began in Paleocene–Eocene time, but major deformation in the Tian Shan appears to have initiated ca. 25 Ma, on the basis of the very sparse data currently available (Hendrix et al., 1994; Sobel and Dumitru, 1997; Yin et al., 1998). Thus, there was a substantial time lag between collision at the southern margin of Asia and the migration of deformation into the Tian Shan. Numerous studies of the Himalaya and Tibet suggest that a major shift from extrusion-dominated to crustal thickening-dominated tectonics occurred in latest Oligocene–early Miocene time, approximately coincident with the start of unroofing in the Tian Shan (e.g., Harrison et al., 1992). This suggests that unroofing in the Tian Shan may have been a distant effect of that shift in tectonic style. Third, Cenozoic deformation has apparently been partitioned into contrasting domains dominated by contraction and strike-slip faulting. Some of this partitioning may reflect the influence and reactivation of preexisting older structures.

The history of deformation in the Tian Shan during the Cenozoic provides a loose analog for the possible effects of earlier Mesozoic collisions at the southern margin of Asia. Specifically, (1) transmission of stresses into the Tian Shan from far distant collisions appears quite plausible, (2) collisions are protracted events (~55–45 m.y. thus far for the India-Asia collision) and so might cause extended episodes of deformation; and (3) there may be significant time lags between the initiation of collision and the initiation of deformation in the Tian Shan. The suture zones from these earlier collisions are preserved within the Himalaya and Tibet (Fig. 1) and are closer to the Tian Shan than the Indus-Tsangpo suture (although still on the opposite side of the Tarim basin) so these collisions might be expected to have had stronger effects on the Tian Shan. On the other hand, the blocks that collided in the Mesozoic were much smaller and less rigid than the Indian subcontinental indenter, which consists primarily of a very large, strong, cold Precambrian craton (Fig. 1).

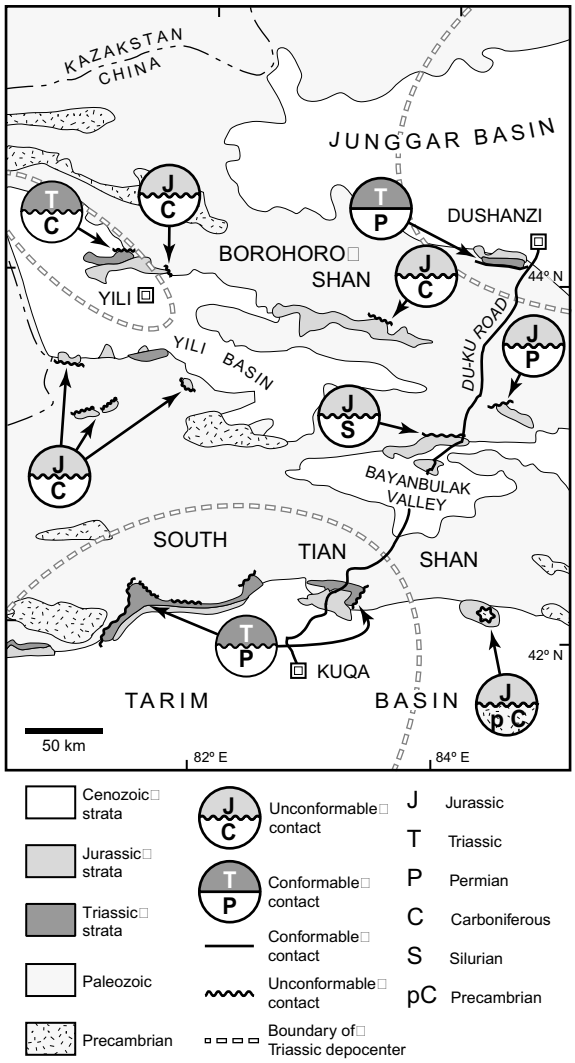

Figure 4. Summary map of depositional contact relations between Jurassic and Triassic strata and underlying Paleozoic and Precambrian rocks in central Tian Shan (Graham et al., 1994), based on Chinese maps (e.g., Chen et al., 1985; Xinjiang Bureau of Geology and Mineral Resources, 1993). Deposition of Jurassic clastic deposits in intermontane basins within several areas on Tian Shan indicates unroofing and exposure of underlying Paleozoic units by Jurassic time. Triassic strata are preserved within core of Yili basin and are overlapped by Jurassic strata. Jurassic strata are unmetamorphosed and generally much less deformed than underlying pre-Mesozoic units. Preservation of Jurassic units is loose indicator that post-Jurassic exhumation has been limited to no more than several kilometers in much of interior of Tian Shan. Yili basin and Bayanbulak Valley are modern intermontane basins within Tian Shan that serve as possible analogs for Mesozoic intermontane basins.

MESOZOIC INTERMONTANE BASINS WITHIN THE TIAN SHAN CORE

Strata in the Tarim and Junggar basins have provided most of the data on the history of the Tian Shan during the Mesozoic. In addition to these strata north and south of the range, large tracts of poorly known Jurassic strata are preserved in intermontane basins within the interior of the range (Figs. 3 and 4) (Xinjiang BGMR, 1985, 1993; Graham et al., 1994; Zhou et al., this volume). These units unconformably overlie strongly deformed Paleozoic rocks (Fig. 4). The most extensive of the intermontane sequences occur in the modern intermontane Turpan basin (Fig. 2) which, on the basis of facies, paleocurrent, and provenance data, was an intermontane basin in Jurassic time, partitioned from the Junggar basin to the north by an ancestral Bogda Shan (Huang et al. 1991; Hendrix et al., 1992; Greene et al., this volume). Within the Tian Shan itself, several smaller areas of Jurassic strata are exposed (e.g., Fig. 3) (Chen et al., 1985; Xinjiang BGMR, 1993; Graham et al., 1994). In one accessible area, strata are tilted ~45° but are otherwise not strongly deformed (Zhou et al., this volume). Preservation of these relatively much less deformed sequences suggests that total post-Jurassic exhumation in these areas has been limited. The modern intermontane basins within the Tian Shan, such as the Yili basin and Bayanbulak Valley (Figs. 2–4), may be localized topographically by Cenozoic reactivation of older structures, and so may provide a rough analog for the older Jurassic basins.

FISSION-TRACK METHODS

General principles

The use of apatite fission-track methods for reconstructing the time-temperature histories of rock samples relies on the facts that new tracks accumulate at an essentially constant rate from the fission decay of trace ^{238}U present within apatite crystals, allowing the calculation of fission-track ages, while at the same time, tracks are partially or totally erased by thermal annealing at elevated subsurface temperatures. Annealing is slight at temperatures $<\sim$60 °C, progressively more severe between about 60 and 110–125 °C, and total at $>$110–125 °C. Total annealing resets the fission-track age to zero, whereas partial annealing reduces the fission-track age and reduces the lengths of individual tracks by amounts directly dependent on the specific temperature (e.g., Naeser, 1979; Gleadow et al., 1986; Green et al., 1989a, 1989b; Dumitru, 2000).

In this study, both primary apatite from plutonic and metamorphic rocks and detrital apatite from sandstones were analyzed (e.g., Dumitru, 2000). The fission-track system records the low-temperature cooling histories of rocks, so ages from plutonic and metamorphic rocks are generally related to final uplift and exhumation of the rocks rather than their earlier igneous crystallization or metamorphism. Data from detrital apatite may yield two different types of information, depending on the maximum paleoburial temperature (T_{max}) undergone by the sandstone sample in question. Where sedimentary horizons were buried to sufficient depth that T_{max} exceeded ~110–135 °C, the fission-track clock is reset to zero age and fission-track data record information on the time-temperature (*t*-*T*) cooling path of the sandstone horizon as it passed through the apatite fission-

track partial annealing temperature window of ~125–60 °C during exhumation (e.g., Green et al., 1989a, 1989b). Assuming a nominal geothermal gradient of 22 °C/km (discussed herein), this is equivalent to unroofing through depths of ~5–2 km below the Earth's surface. With shallower burial at $T_{max} <$~50 °C, detrital apatites in sandstones instead retain fission-track ages of their sediment source areas. Such ages generally date cooling of rocks in the source area, such as following igneous activity or exhumation (e.g., Cerveny et al., 1988), and different apatite grains within a given sample may yield different ages if they were derived from different source areas. In the current study, shallowly buried samples yielded late Paleozoic, Mesozoic, and Oligocene–Miocene provenance ages and thus constrain cooling in sediment source areas during those times. Where T_{max} was between about 50 and 125 °C, the fission-track clock is partially reset, and interpretation of data patterns permits less precise estimates of provenance ages and cooling ages.

Interpretation of fission-track data involves the analysis of several fission-track parameters in addition to the sample fission-track age. Track length data are useful because lengths of individual tracks are shortened during partial annealing by an amount directly dependent on the temperature. Because new tracks are continuously formed over geologic time, each track formed at a different time and therefore existed to respond and shorten during a different portion of the total thermal history of the sample. A moderate heating event (e.g., 90 °C) occurring 75% of the way through a sample's history, for example, will shorten the 75% of the tracks formed before the event but will not affect the 25% of the tracks formed after the heating. The distribution of track lengths, generally measured as a histogram of the lengths of 100–150 individual tracks, therefore records details of the *t-T* path. In the case just mentioned, 75% of the tracks in the histogram will be short and 25% will be long (ignoring certain biasing factors). This *t-T* information may be recovered by modeling of the time-constant track production and temperature-dependent track annealing processes to determine the spectrum of *t-T* paths consistent with the observed age and track length data (e.g., Green et al., 1989a; Corrigan, 1991; Gallagher, 1995).

Single-grain age data are useful because different apatite grains in a sample may anneal at somewhat different temperatures, a kinetic effect related to the differing chemical composition of the grains. Thus exposure to certain temperatures (~95–125 °C in most cases) may totally anneal some grains and reset their ages to zero, while other grains are only partially annealed. In this case, ages of the youngest, totally reset grains may date exhumation and cooling (e.g., Green et al., 1989a; Sobel and Dumitru, 1997).

Figure 5 illustrates expected idealized fission-track data patterns for *t-T* histories where sediments are eroded from a source terrane, deposited, buried, and heated in a sedimentary basin, then exhumed back to the surface during an unroofing event. In path A, the sample was only shallowly buried in the basin at a maximum burial temperature (T_{max}) of 30 °C. At these low burial temperatures, annealing is minimal and all track lengths remain long and the sample retains the fission-track age of a cooling event in the sediment source area. Figure 5 assumes that all grains were derived from a single source area of uniform apatite age, and the single-grain ages for path A cluster within a $\pm 2\sigma$ swath on a radial plot (see Fig. 5) that records this provenance age. If grains were derived from multiple sources with different ages, there would be a spread in ages reflecting this, but all age clusters would be at least as old as the depositional age of the sediment. As burial depths and T_{max} increase (Fig. 5, paths B and C, 60–85 °C), track lengths shorten and the apparent sample age becomes younger. In path D (100 °C), the track length distribution becomes bimodal. The bimodality is due to combining a component of early formed tracks that have been strongly shortened by burial heating with a component of long tracks that formed after the sample cooled. Single-grain ages are widely spread in a distinctive mixed age wedge. The youngest age component approximates the cooling age because it includes grains that were totally annealed before cooling (generally, the more F-rich grains), whereas the oldest age component (Cl-rich grains) approaches the original provenance age. With even deeper burial (path E, 115 °C), length distributions are dominated by long tracks formed after maximum temperatures because most of the older, shortened tracks have been totally erased. Single-grain ages still show a broad spread, but the young cluster is dominant. Finally, when T_{max} exceeds ~125 °C (path F), all tracks formed before cooling are totally erased. Length distributions are long again, because all preexhumation tracks have been completely erased. If cooling is fairly rapid, all single-grain ages will cluster within a $\pm 2\sigma$ swath and date the time of cooling.

Analytical methods

Laboratory procedures used in this study were essentially identical to those used by Dumitru et al. (1995, their Table 2) and are summarized in the footnote to Table 1. For track length analyses, 100–150 horizontal confined tracks (Laslett et al., 1982) were measured in each sample, provided that many were present. For age determinations, 20–40 good-quality grains per sample were dated, again assuming that sufficient grains were present. Following convention, all statistical uncertainties on ages and mean track lengths are quoted at the $\pm 1\sigma$ level, but $\pm 2\sigma$ uncertainties are taken into account for geologic interpretation. Maximum burial paleotemperatures of sandstone samples were estimated using the methods of Dumitru (1988). For samples that yielded good quality track length data and relatively tightly clustered single-grain age distributions, the 1998 version of the Monte Trax fission-track modeling program of Gallagher (1995) was used to determine the spectrum of time-temperature histories consistent with the observed age and track length data. The footnote of Table 1 lists the specific modeling parameters use.

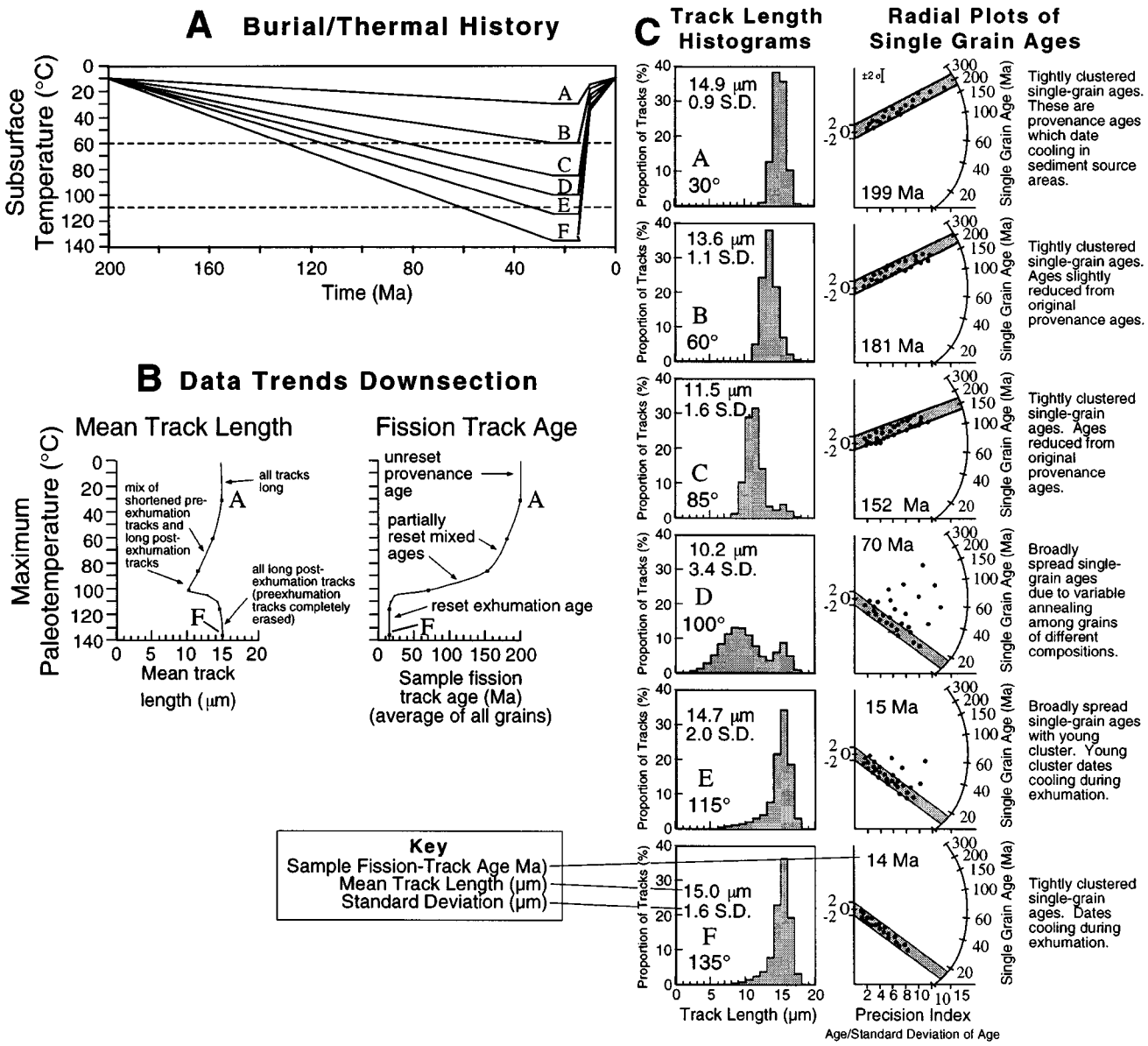

Figure 5. A: Hypothetical burial, exhumation, and thermal histories for sedimentary basin. B: Idealized fission-track age and mean track length trends versus depth in section for thermal histories in A. C: Idealized track length histograms and single-grain age distributions for these thermal histories (Sobel and Dumitru, 1997; see also Dumitru, 2000). Single-grain age distributions are displayed on radial plots, special plots developed to accommodate large and widely varying statistical uncertainties on single-grain ages (Galbraith, 1990; Galbraith and Laslett, 1993; see also Dumitru, 2000). In these plots, individual grain ages are read by projecting line from plot origin (0) through each data point onto radial age scale. Key features of radial plots are that all grain ages have error bars of equal length (one example is shown in plot for path A) and more precise single-grain ages plot farther to right. If all grains have statistically concordant ages, data points cluster within $\pm 2\sigma$ swath (e.g., A, B, C, F). If there are significant differences between ages of individual grains, points scatter outside of single swath (e.g., D, E). See text for description of systematic data trends.

TABLE 1. FISSION TRACK SAMPLE LOCALITY, COUNTING, AND AGE DATA

Sample number	Irradiation number	Latitude (°N)	Longitude (°E)	Elevation (m)	No xls	Spontaneous		Induced		$P(\chi^2)$ (%)	Dosimeter		Age $\pm 1\sigma$ (Ma)
						Rho-S	NS	Rho-I	NI		Rho-D	ND	
Manas Samples*													
M1 (89-M-52)	SU002-17	42°58′30″	85°49′20″	1160†	22	1.2380	632	2.2440	1145	12.0	1.7920	7838	186.9 ± 10.0
M2 (89-M-44)	SU002-16	43°56′40″	85°51′50″	1160†	20	0.7480	355	2.5910	1229	0.7	1.7920	7838	97.6 ± 9.9
M3 (89-M-30)	SU002-15	43°55′10″	85°52′40″	1160†	39	0.4270	452	5.2180	5591	<0.1	1.7920	7838	32.5 ± 5.3
M4 (89-M-14)	SU002-14	43°51′50″	85°49′40″	1160†	37	0.3910	977	3.2320	8080	<0.1	1.7920	7838	38.1 ± 4.0
M5 (89-M-7)	SU002-12	43°51′20″	85°49′00″	1160†	16	0.1800	92	2.2790	1170	0.3	1.7920	7838	29.7 ± 5.7
Aksu Samples													
91-SI6	SU016-04	40°48.3′†	79°50.2†	1370†	41	0.4140	586	0.5207	737	58.0	1.4990	4116	226 ± 13
91-SU1	SU016-05	40°48.3′†	79°50.0†	1370†	21	1.3960	913	1.7100	1119	<0.1	1.4920	4116	240 ± 21
91-SU2	SU016-06	40°50.4′†	79°52.7†	1370†	16	2.2630	803	2.9650	1052	<0.1	1.4920	4116	211 ± 16
91-SH5	SU016-08	40°50.4′†	79°52.7†	1370†	16	1.5240	1000	2.3120	1517	0.2	1.4850	4116	185 ± 12
91-SH6	SU016-09	40°50.4′†	79°52.7†	1370†	20	1.1200	1090	1.3450	1309	<0.1	1.4780	4116	238 ± 17
91-SI4	SU006-09	40°54.9′†	79°54.1†	1370†	33	0.8721	1476	1.1980	2027	<0.1	1.5830	4534	222 ± 12
91-SH2	SU006-08	40°55.1′†	79°50.8†	1370†	14	0.6619	379	0.8505	487	1.8	1.5870	4534	219 ± 23
91-SU8	SU006-14	40°55.1′†	79°50.8†	1370†	12	2.1170	986	3.6980	1722	0.4	1.5620	4534	168 ± 11
Kuqa Samples													
K-1(89-K-115)	SU002-22	42°06′30″	83°06′00″	1980†	20	0.7999	535	3.1340	2096	<0.1	1.7920	7838	103.3 ± 16.0
K-2(89-K-34-38)	SU002-20	42°08′30″	83°06′50″	1980†	10	1.4420	272	2.4920	470	44.0	1.7920	7838	197.1 ± 15.0
K-3(89-K-113)	SU002-21	42°09′30″	83°06′30″	1980†	20	0.5195	202	3.5260	1371	5.0	1.7920	7838	50.0 ± 4.4
K-4(89-K-17B)	SU002-19	42°14′20″	83°14′00″	1980†	13	1.3480	224	5.0290	836	1.0	1.7920	7838	96.7 ± 12.0
K-5(89-K-15)	SU002-18	42°14′30″	83°14′30″	1980†	20	0.4523	368	1.8210	1482	0.2	1.7920	7838	96.7 ± 9.3
K-6(89-K-118)	SU002-23	42°15′30″	83°15′20″	1980†	20	0.7312	499	3.7540	2562	0.1	1.7920	7838	67.1 ± 5.5
K-7(89-K-1)	SU014-35	42°17′20″	83°16′30″	1980†	20	0.5300	574	1.5370	1664	4.4	1.3050	4064	86.3 ± 5.4
Du-Ku Samples													
DK21 (Dom. K)	SU023-04	44°05.0′	84°42.1′	1220	19	0.1705	115	0.2431	164	8.7	1.7090	5073	227.2 ± 28.0
DK23 (Dom. J)	SU023-06	43°46.0′	84°28.1′	2800	35	0.2750	212	2.3650	1823	2.0	1.7300	5073	38.7 ± 3.5
DK24 (Dom. J)	SU023-07	43°46.0′	84°28.1′	2800	48	0.0361	97	0.7999	2147	0.2	1.7510	5073	15.3 ± 2.1
DK25 (Dom. J)	SU023-08	43°45.7′	84°27.0′	3360	38	0.0782	137	0.8233	1443	3.5	1.7510	5073	32.0 ± 3.5
DK26 (Dom. J)	SU023-09	43°44.6′	84°26.2′	3200	36	0.1461	323	1.7440	3855	0.8	1.7720	5073	28.6 ± 2.2
DK27 (Dom. J)	SU023-10	43°44.4′	84°25.5′	3440	25	0.3967	563	11.2800	16013	94.0	1.7720	5073	12.0 ± 0.5
DK28 (Dom. J)	SU023-11	43°44.4′	84°25.5′	3440	31	0.0479	58	1.5490	1875	31.0	1.7930	5073	10.7 ± 1.4
DK29 (Dom. J)	SU023-12	43°43.8′	84°25.8′	3760	29	0.3168	481	4.6860	7116	35.0	1.7930	5073	23.4 ± 1.1
DK30 (Dom. J)	SU023-14	43°43.7′	84°25.3′	3480	24	0.2402	241	3.7640	3776	47.0	1.8250	5073	22.4 ± 1.5
DK32 (Dom. I)	SU023-15	43°43.2′	84°25.9′	2920	29	0.7804	811	2.5680	2669	34.0	1.8250	5073	106.1 ± 4.5
DK33 (Dom. I)	SU023-16	43°42.4′	84°27.0′	3080	36	0.8339	2042	2.6030	6373	0.1	1.8460	5073	113.1 ± 4.4
DK34 (Dom. H)	SU023-17	43°39.4′	84°19.4′	2560	38	0.3542	198	0.7174	401	0.5	1.8460	5073	173.5 ± 21.0
DK36 (Dom. G)	SU023-18	43°30.6′	84°27.4′	3010	15	0.0686	12	1.0860	190	61.0	1.8670	5073	22.7 ± 6.8
DK37 (Dom. G)	SU023-19	43°29.5′	84°27.1′	3280	5	0.0234	2	0.9235	79	8.3	1.8670	5073	9.1 ± 6.5

TABLE 1. FISSION TRACK SAMPLE LOCALITY, COUNTING, AND AGE DATA (continued)

Sample number	Irradiation number	Latitude (°N)	Longitude (°E)	Elevation (m)	No xls	Spontaneous		Induced		$P(\chi^2)$ (%)	Dosimeter		Age $\pm 1\sigma$ (Ma)
						Rho-S	NS	Rho-I	NI		Rho-D	ND	
DK41 (Dom. G)	SU023-20	43°28.6′	84°27.0′	3360	9	0.9919	162	10.0800	1646	38.0	1.8880	5073	35.8 ± 3.0
DK43 (Dom. F)	SU023-21	43°23.2′	84°23.2′	2400	24	2.1250	2467	3.1070	3606	43.0	1.8880	5073	244.5 ± 7.3
DK44 (Dom. F)	SU023-22	43°23.0′	84°23.2′	2280	11	2.1420	610	3.7250	1061	85.0	1.9090	5073	208.3 ± 11.0
DK45 (Dom. F)	SU023-23	43°17.4′	84°18.9′	1760	25	1.4210	2835	1.8600	3710	84.0	1.9090	5073	275.4 ± 7.9
DK52 (Dom. E)	SU034-13	43°11.3′	84°17.3′	2560	28	0.3795	839	0.9857	2179	75.0	1.7030	4808	125.3 ± 5.4
J4 (Dom. E)	SU034-12	43°11.3′†	84°17.3′†	2560†	11	1.5650	566	3.7500	1356	2.6	1.7030	4808	135.7 ± 9.7
J5 (Dom. E)	SU034-15	43°11.3′†	84°17.3′†	2560†	14	0.3879	399	1.1660	1199	6.4	1.7330	4808	110.3 ± 6.6
J9 (Dom. E)	SU034-16	43°11.1′†	84°17.4′†	2600†	10	1.4500	719	4.5320	2247	44.0	1.7330	4808	106.1 ± 4.8
DK53 (Dom. E)	SU034-11	43°10.9′	84°17.6′	2640	5	0.3858	57	1.7600	260	60.0	1.6830	4808	70.8 ± 10.0
J12 (Dom. E)	SU034-10	#	#	#	5	0.1923	43	0.4204	94	0.6	1.6830	4808	146.9 ± 52.0
DK55 (Dom. D)	SU034-09	43°00.1′	84°09.8′	2710	25	1.5440	2108	2.3800	3248	1.3	1.6630	4808	204.9 ± 8.4
DK61 (Dom. D)	SU023-24	42°59.9′	84°08.9′	2660	21	1.0660	1128	1.9890	2104	34.0	1.9300	5073	196.6 ± 7.8
DK62 (Dom. C)	SU023-25	42°32.7′	83°33.6′	2960	2	0.5675	16	1.3120	37	16.0	1.9300	5073	159.0 ± 48.0
DK68 (Dom. B)	SU023-26	42°19.7′	83°11.7′	2000	15	0.3415	84	2.4400	600	30.0	1.9400	5073	52.2 ± 6.1

Note: Abbreviations are: No xls—number of individual crystals (grains) dated; Rho-S—spontaneous track density ($\times 10^6$ tracks per square centimeter); NS—number of spontaneous tracks counted; Rho-I—induced track density in external detector (muscovite) ($\times 10^6$ tracks per square centimeter); NI—number of induced tracks counted; $P(\chi^2)$ – χ^2 probability (Galbraith, 1981; Green, 1981); Rho-D—induced track density in external detector adjacent to dosimetry glass ($\times 10^6$ tracks per square centimeter); ND, number of tracks counted in determining Rho-D. Age is the sample central fission-track age (Galbraith and Laslett, 1993), calculated using zeta calibration method (Hurford and Green, 1983). Analyst: T.A. Dumitru.

The following is a summary of key laboratory procedures. Apatites were etched for 20 s in 5N nitric acid at room temperature. Grains were dated by external detector method with muscovite detectors. Samples were irradiated in well thermalized positions of Texas A&M University (SU002, SU006) or Oregon State University (SU014, SU016, SU023, SU034) reactor. CN5 dosimetry glasses with muscovite external detectors were used as neutron flux monitors. External detectors were etched in 48% HF. Ttacks counted with Zeiss Axioskop microscope with 100× air objective, 1.25× tube factor, 10× eyepieces, transmitted light with supplementary reflected light as needed; external detector prints were located with Kinetek automated scanning stage (Dumitru, 1993). Only grains with c axes subparallel to slide plane were dated. Ages calculated using zeta calibration factor of 389.5. Confined tracks lengths were measured only in apatite grains with c axes subparallel to slide plane; only horizontal tracks measured (within ±~5°-10°), following protocols of Laslett et al. (1982). Lengths were measured with computer digitizing tablet and drawing tube, calibrated against stage micrometer (Dumitru, 1993). Data reduction was done with program by D. Coyle.

Summary of thermal history modeling methods: modeling done with February 11, 1998 version of "code_trax" program, an updated version of the Monte Trax program of Gallagher (1995). Modeling parameters used: (1) used raw track length data (actual lengths of each track) and actual track counts (NS and NI for each grain), (2) used ±10% uncertainty on observed age, ±0.35 micron uncertainty on mean length, and ±0.5 micron uncertainty on standard deviation of track length distribution, (3) used least likelihood evaluation method, (4) used initial track length of 16.3 microns, (5) used Durango apatite annealing model of Laslett et al. (1987), (6) modeled with 100 simulated tracks and 500 to 2000 Monte Carlo runs (genetic algorithm not used), (7) output plots show all runs which pass least likelihood test for both age and track length data.

*Previously published in Data Repository form by Hendrix et al. (1994).

†Approximate location and/or elevation.

#Location unknown. Approximate location shown in cross section of Zhou et al. (this volume).

Geothermal gradients

Fission-track data constrain time-temperature histories and it is desirable to convert these into time-depth histories. If the geothermal gradient is constant, this is straightforward. However, gradients vary over time and in response to rapid burial and exhumation events. In this chapter a paucity of constraints on the thermal history over the past 300 m.y. forces us to simply assume a nominal constant geothermal gradient of 22 °C/km and a surface temperature of 10 °C, based on limited available data on Cenozoic thermal gradients in basins in the region (Zhang, 1989; Fan et al., 1990; see also Sobel and Dumitru, 1997). These are fairly typical values based on worldwide geothermal gradient and heat-flow data sets (e.g., Turcotte and Schubert, 1982).

FISSION-TRACK DATA

Figure 2 shows the locations of the fission-track sampling areas. We first summarize previously published data from the Manas section on the northern flank of the Tian Shan. The interpretation of this area is especially straightforward and serves as a model for the interpretation of results from other areas. We then present results from other areas, proceeding generally from southwest to northeast.

It is useful to keep several points in mind in reading these descriptions. First, the apatite fission-track system is sensitive to cooling only within a temperature window of about 60–125 °C, so cooling events outside this range are not recorded. Second, samples from different burial depths within a single section may cool through the fission-track temperature sensitivity window at different times, so apparent fission-track ages of samples from a single area may be expected to vary substantially. Third, later exhumation and cooling events tend to overprint and erase the fission-track evidence of earlier events. Thus earlier events certainly affected broader areas than revealed by the fission-track data, but fission-track evidence is only retained in areas not subjected to large amounts of younger overprinting deformation and exhumation.

Manas section, southern margin of Junggar basin

The Junggar basin is the major Mesozoic–Cenozoic foreland basin north of the Tian Shan (Figs. 1–3). Its main depocenter lies immediately adjacent to the Tian Shan, where it is ~11 km thick and has been upturned and exposed along the northern flank of the range (Hendrix et al., 1992). Hendrix et al. (1994) reported fission-track data from five Junggar sandstone samples exposed in a north-dipping homoclinal section in the Manas River valley (Fig. 6; Table 1). The data display the overall pattern of younger sample fission-track age with increasing paleodepth and paleotemperature that is expected from increased annealing structurally downsection (Fig. 6B).

In the shallowest sample (M1), single grain ages are tightly clustered ca. 186 Ma and are much older than the sandstone's depositional age (ca. 80 Ma) (Fig. 6C). Individual grains in sandstones commonly have a range of annealing susceptibilities (correlated with apatite composition), and the lack of any grains significantly younger than the depositional age indicates only slight thermal annealing at burial temperatures $<$~85–90 °C (Green et al., 1989a). M1 has a tight track-length distribution with a mean track length of 12.4 μm, shorter than the 14.5–15.5 μm lengths in samples exposed only to near-surface temperatures (Gleadow et al., 1986; Green et al., 1989b). A tight distribution with a mean length of ~12.4 μm and few tracks longer than 14 μm suggests exposure to burial temperatures of ~60–90 °C late in the sample's history, after most of the tracks had formed (Green et al., 1989a, 1989b; Corrigan, 1993). These observations suggest that M1 was buried ~2.3–3.6 km (assuming a 22 °C/km gradient) sometime in the middle or late Cenozoic, before being exhumed to the surface.

In sample M2, about one-half of the single-grain ages are distinctly younger than the depositional age, whereas the remainder are about as old as the depositional age. The mean track length is 11.9 μm. These observations suggest partial annealing at maximum burial temperatures of ~80–100 °C. The track-length distribution is tight, and few tracks are longer than 13 μm, so cooling occurred sometime in the middle or late Cenozoic, after most of the tracks had formed.

The three deepest samples (M3, M4, M5) have much younger, middle Tertiary sample apparent fission-track ages. The radial plots of single-grain ages indicate that these samples have been strongly but not totally annealed. The plots show pronounced clusters of young grains ca. ~25 Ma, with no significantly younger grains, but with small proportions (~10%–25%) of much older grains. This single-grain age pattern indicates exposure to temperatures of ~95–120 °C (paleodepths of ~4–5 km) ca. 25 Ma, sufficient to anneal fully all but the most retentive grains (e.g., Green et al., 1989a, 1989b; Dumitru, 2000). The broad track-length distributions with numerous short tracks are further evidence that annealing was not total. Cooling of the samples to temperatures below ~80–95 °C ca. 25 Ma is indicated by the resetting of most of the single-grain ages at that time.

An age of 24.7 $\pm$ 3.8 Ma ($\pm 1\sigma$) for the young clustering of grains was calculated from the combined data from samples M3–M5 (Sobel and Dumitru, 1997, their Table 3), and is the best estimate of the time significant cooling and exhumation began. The amount of unroofing and cooling at this time is only roughly constrained. The samples probably cooled at least 10–20 °C to set the tight cluster of ca. 25 Ma grains, equivalent to at least 0.5–1 km of unroofing. The similarity in cooling age over the 12 km map distance between M3 and M5 suggests that the unroofing was a strong event and thus significantly greater than 0.5–1 km. The total amount of ca. 25 Ma to Holocene unroofing of M3–M5 was ~4–5 km, and the rugged modern topography and active seismicity of the Tian Shan suggest that a significant part of this total occurred in the latest Cenozoic, well after 25 Ma.

The Monte Trax program (Gallagher, 1995; see also footnote to Table 1) was used to model the fission-track data from

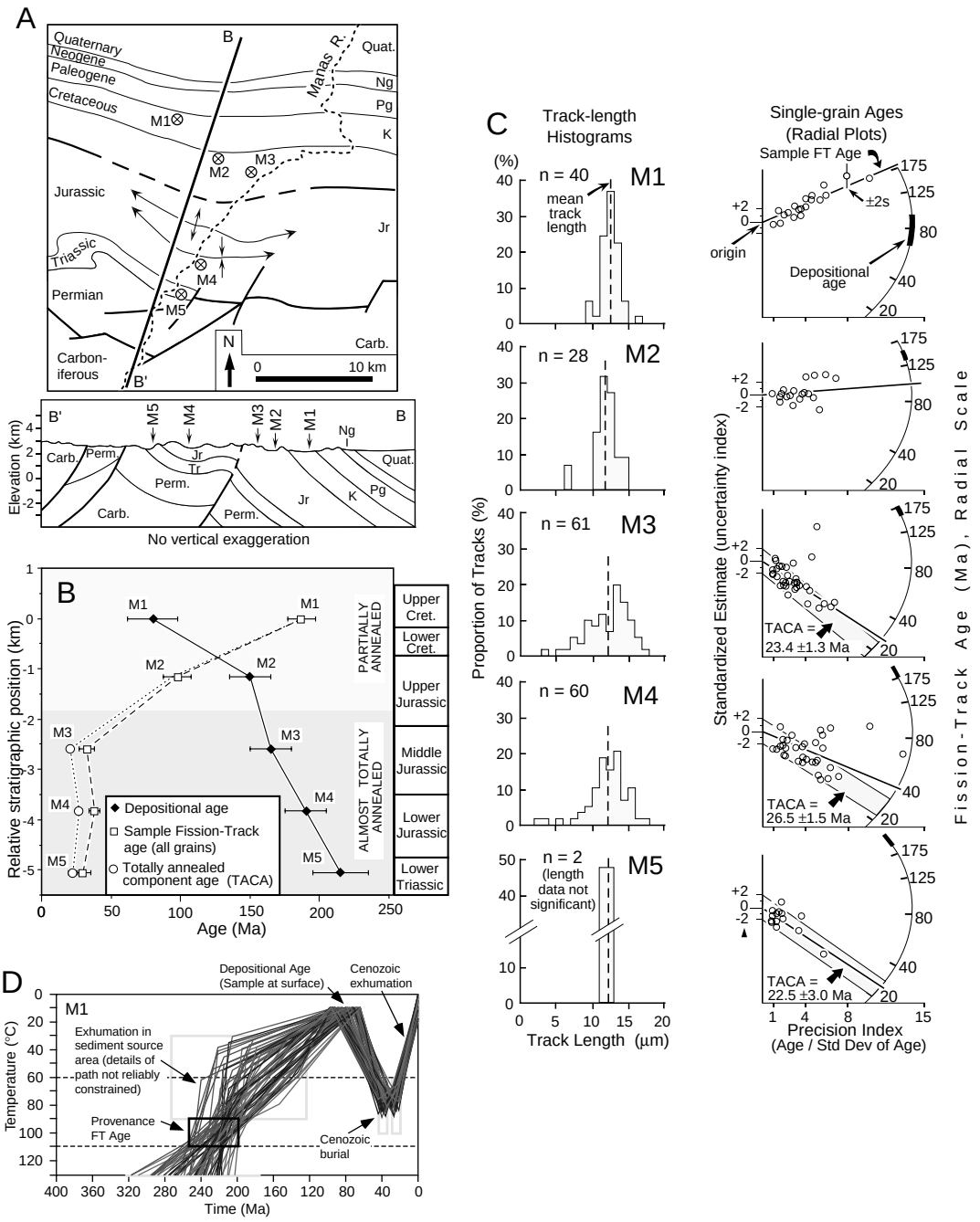

Figure 6. A: Map and cross section of Manas River section on northern flank of Tian Shan, based on unpublished Chinese maps and Hendrix et al. (1992). B: Plot of sample fission-track (FT) ages versus relative stratigraphic depth in section, showing systematic reduction in age with increasing depth. C: Fission-track length histograms and radial plots of single-grain fission-track ages. Note strong clustering of single grain ages ca. 25 Ma in three deepest samples, where shaded $\pm 2\sigma$ swath denotes grains that were totally annealed before cooling ca. 25 Ma. These samples also contain small numbers of much older grains that had not been totally reset to zero age at 25 Ma. These data are interpreted to indicate that unroofing in this area initiated ca. 25 Ma, before which time deepest sample was buried at depth of ~5 km and temperature of ~100–125 °C. Figure is modified from Hendrix et al. (1994). Ages of totally annealed components calculated in Sobel and Dumitru (1997; Table 3). D: Modeling of fission-track data from Cretaceous sandstone sample M1. All paths shown are compatible with observed data. Modeling indicates cooling below ~100 °C in sediment source areas at 200–250 Ma. Note that although model plots extend to temperatures of 130 °C, histories hotter than about 110 °C cannot normally be constrained by fission-track data. Therefore specific cooling paths through 130–110 °C temperature interval should not be relied upon.

sample M1. Figure 6D shows the family of thermal histories that are compatible with the observed age and track length data. The depositional age of M1 is Cretaceous, and the modeling indicates cooling below ~100 °C at 200–250 Ma. This suggests that significant cooling occurred in the sediment source area(s) for the detrital apatite in M1 at that time, suggesting exhumation and deformation in source areas at about that time.

Wenguri section, southern Tian Shan thrust belt

The modern boundary between the Tian Shan and the Tarim basin is formed by the southern Tian Shan thrust belt, which extends east-west for about 1200 km (Fig. 2). Yin et al. (1998) divided the belt into four segments, based on differences in structural style. We have fission-track data from four locations along the belt.

Sobel and Dumitru (1997) reported data from sections near Wenguri and Kuzigongsu on the northwest margin of the Tarim basin (Fig. 2). The samples are Jurassic, Cretaceous, and Miocene sandstones of the Tarim basin section that have been uplifted and exhumed by erosion following late Cenozoic folding and thrusting in the area. This shortening is presumably a result of the India-Asia collision and has affected large areas around the northwestern and southwestern margins of the Tarim basin (Sobel and Dumitru, 1997).

At Wenguri, two samples of Cretaceous strata (W5 and W6 in Fig. 7A) show sample ages of 141 ± 13 and 155 ± 11 Ma. Almost all single-grain ages are tightly clustered and are older than the depositional age, indicative of a provenance age. Mean track lengths are 10.9 and 11.5 μm, suggesting burial at maximum temperatures of 80–90 °C; late Cenozoic cooling below ~60 °C is indicated by the low proportion of long tracks (e.g., Green et al., 1989b). These burial temperatures have reduced the fission-track ages. Modeling with the Monte Trax program of Gallagher (1995) corrects for this and yields a provenance age of ca. 160–250 Ma (Fig. 7B), suggesting cooling below ~100 °C in the sediment source area at that time.

In contrast to the Cretaceous samples, four samples of Miocene strata (W1–W4) show widely spread single-grain ages ranging from similar to the Miocene depositional ages to 100–200 Ma. The radial plots show that there are distinct clusters of young grains similar in age or only slightly older than the respective depositional ages (Fig. 7A). The ages of these young clusters decrease upsection. The older populations of grains are less well defined but are generally consistent with the provenance ages of the two Cretaceous samples discussed herein. All of these grains record provenance ages (Sobel and Dumitru, 1997).

These data indicate that unroofing in at least one sediment source area cooled rocks through ~100 °C (and subsequently exposed them at the surface) from at least Oligocene–Miocene time (23.5 ± 3.9, 25.0 ± 3.9 Ma) to middle Miocene time (16.9 ± 2.7, 13.1 ± 2.2 Ma) (Fig. 7A). The source areas may be areas to the north and east in the Tian Shan that are cut by southvergent Neogene thrust faults (Wang et al., 1992). The older grains may be derived from other source areas or from higher structural levels within the same source areas.

The modeled provenance age of the two Cretaceous samples is ca. 160–260 Ma and the Miocene samples also contain an old population of apatite generally compatible with this age. Paleocurrent indicators in the Cretaceous section suggest sediment transport from the east (Sobel and Dumitru, 1997). The Bachu uplift (Fig. 2) separated the north Tarim and southwest Tarim basins from the Triassic until the Miocene (e.g., Carroll et al., this volume). Therefore sediment was likely derived from parts of the Tian Shan north and west of Bachu. To the east, in north Tarim, the sedimentary record suggests an episode of Late Triassic–Early Jurassic deformation (Hendrix et al., 1992) that may have set these provenance ages.

Kuzigongsu section, southern Tian Shan thrust belt

Ten samples were analyzed from Jurassic to Paleogene strata near the Kuzigongsu River (Sobel and Dumitru, 1997). The deepest Jurassic sample yielded the most informative data (Fig. 7C). In this sample, almost all grains clustered at an age of 13.6 ± 2.2 Ma, with a few older grains. This indicates cooling of the sample from a T_{max} of 105–130 °C ca. 14 Ma. Southvergent thrusts south of the section may have accommodated the exhumation.

Kalpin (Aksu) uplift, southern Tian Shan thrust belt

The Kalpin uplift is a large belt of southeast-vergent folding and thrusting of Cenozoic age that has exposed large tracts of Paleozoic strata and lesser tracts of older units along the southern margin of the Tian Shan (Figs. 2 and 8) (McKnight, 1993, 1994; Carroll et al., 1995, this volume; Yin et al., 1998; Allen et al., 1999). The section in the general area consists of upper Proterozoic basement unconformably overlain by upper Proterozoic to Upper(?) Permian strata. The Permian strata are in turn overlain along a major angular unconformably by Neogene to Quaternary strata. The upper Proterozoic to Permian section constitutes a passive margin succession deposited on the northern margin of the Tarim block. In most areas the thrust style is thin skinned with a decollement within Cambrian strata. In the southern part of the belt, the stratigraphic thicknesses of the passive margin units in the thrust sheets are nearly constant and the thrusts are very regularly spaced at about 12–15 km, suggesting that folding instability controlled the thrust architecture (Yin et al., 1998).

We collected 11 samples from two eroded homoclines near Aksu that presumably are cored by buried Cenozoic thrust faults (Fig. 8A). One of these samples is from Neogene clastics, the rest are from Sinian (late Precambrian) to Permian units. The structural style near Aksu is somewhat different than the regularly spaced thrust imbricates farther to the west. There is apparently no decollement within the Cambrian strata, and thick

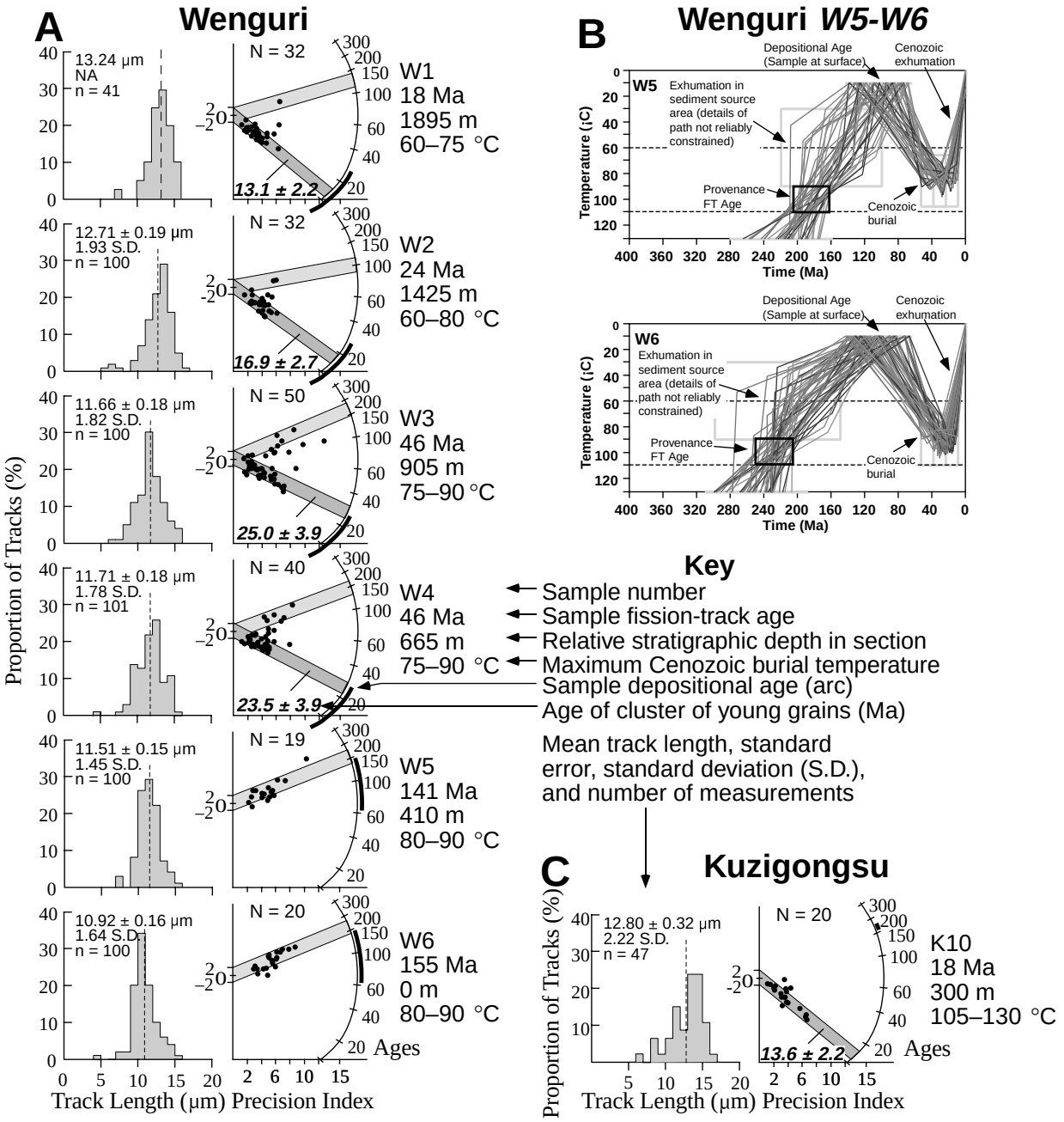

Figure 7. A: Fission-track data from Wenguri section on southern flank of Tian Shan. None of these samples have been buried deeply enough to strongly anneal fission tracks in apatite. Four shallowest samples are Miocene sandstones where most apatite grains yield single grain ages only slightly older than Miocene depositional ages, but there are also small numbers of much older grains. Note that young grains trend younger upsection, tracking depositional age trend. These samples record provenance fission-track information, indicating major unroofing in sediment source areas in Miocene time. Older grains were derived either from higher levels within these source areas or from other source areas with more limited Miocene unroofing. Two deepest samples are Cretaceous sandstones. All grains are older than depositional ages, indicating that these samples underwent only limited burial (estimated maximum burial temperatures of 80–90 °C). B: Modeling of two deepest samples, indicating provenance age of ca. 160–260 Ma. C: Data from stratigraphically deepest sample in Kuzigongsu section on southern flank of Tian Shan. This sample has Jurassic depositional age. Only this sample was sufficiently buried to reset most of grains. Note strong clustering of grains at 14 Ma (with a few older grains), indicating major cooling ca. 14 Ma. See Sobel and Dumitru (1997) for maps, cross sections, and data from additional partially reset samples from shallower in Kuzigongsu section.

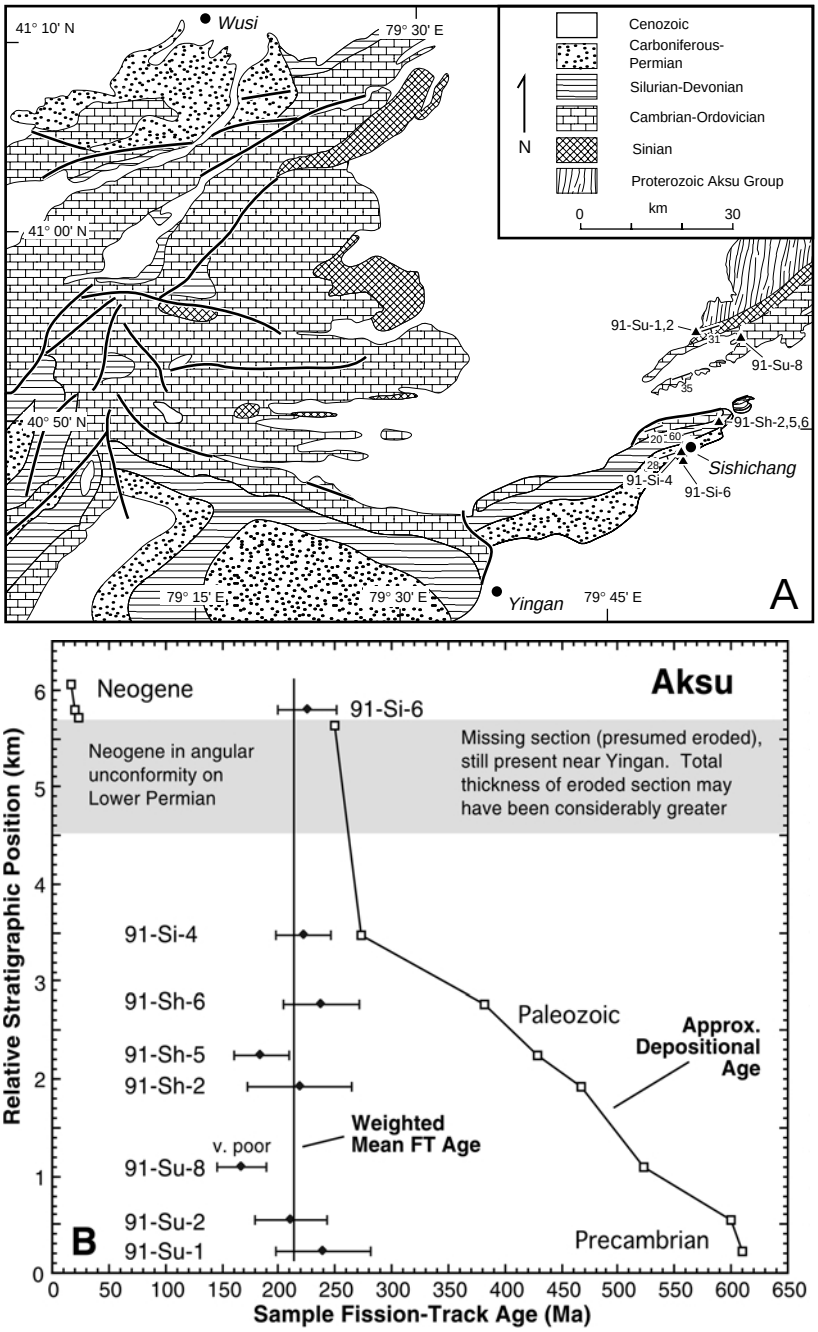

Figure 8. A: Geologic map of Aksu area on southern flank of Tian Shan, showing sampling localities. Map modified from unpublished 1:200 000 mapping by Xinjiang Bureau of Geology and Mineral Resources, Gao et al. (1985), and Carroll et al. (1995, this volume). B: Plot of fission-track ages vs. relative stratigraphic position in section. Note essentially constant ages through entire section. C (following page): Radial plots and track length histograms. Five samples labeled M yielded sufficient length data to permit modeling (see Fig. 9).

sections of Precambrian strata are involved in the folding (e.g., Liou et al., 1989).

The quality of the apatite in these samples proved to be poor and only eight samples yielded usable data. Sample ages are approximately constant through the section (ca. 214 Ma), and we infer that irregular variations in age within the section probably reflect minor errors induced by the poor sample quality rather than true variations in cooling histories (Fig. 8). In order to filter out some of this variation, we calculated a weighted mean age of 214 ± 6 Ma for six of the samples, excluding sample SU-8, which had very poor quality apatite, and the Neogene sample. Useful track length data could be collected from five of the samples (Fig. 8C).

We used the Monte Trax program to model the histories of these five samples twice, first using the actual measured fission-track ages for each sample and second using the 214 Ma mean age, which is probably a better estimate of the true age. The modeling indicates major cooling of all samples through the 100 °C isotherm ca. 250 ± 10 Ma (Fig. 9), i.e., in latest Paleozoic time. The youngest Paleozoic strata in the area, which are

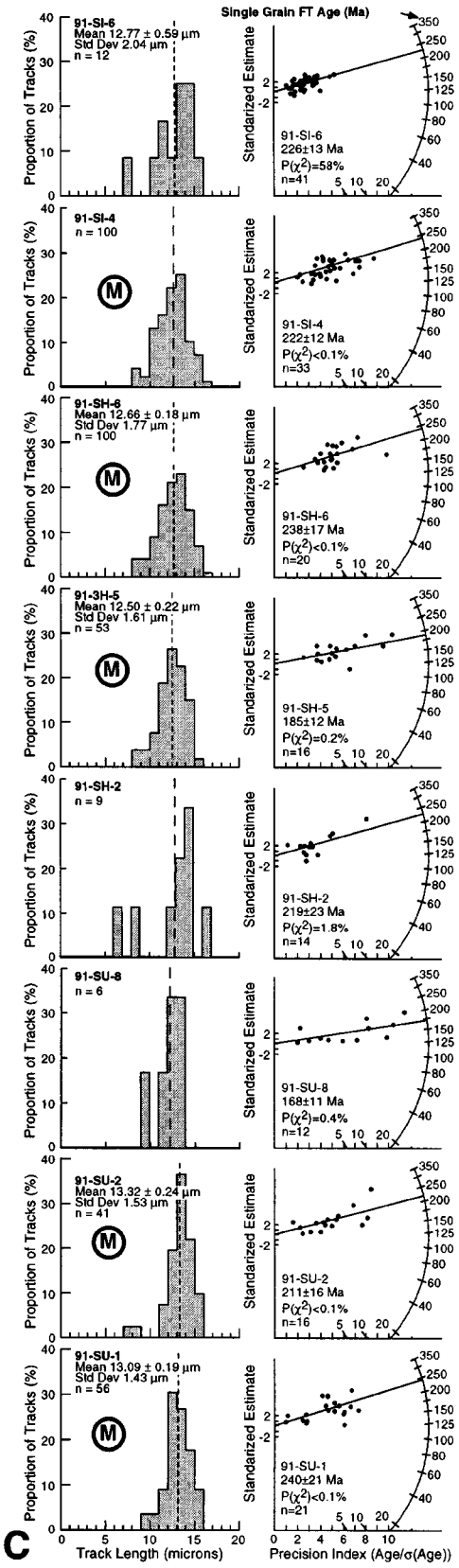

Figure 8. (*continued*)

nonmarine clastics, have generally been assigned an Upper Permian age (256–245 Ma on the time scale of Harlan et al., 1990) based on lithologic correlations, although no definitive data support this, and they could be Lower Permian (e.g., Carroll et al., this volume). In either case, cooling apparently began soon after the termination of deposition in the area.

The stratigraphically deepest sample SU-1 illustrates most aspects of the overall uplift history. Stratigraphic reconstructions suggest that this sample was buried about 7.5 km in middle Permian time (ca. 260 Ma) (Carroll et al., this volume). The fission-track data indicate major cooling beginning ca. 250 Ma (±10 m.y.) to temperatures of ~60–80 °C, corresponding to depths of about 1–3 km assuming a geothermal gradient between 22 and 50 °C/km (see following). Thus total unroofing of about 5 km in early Mesozoic time is indicated. All the other samples show similar unroofing but of lesser magnitude, because the initial preunroofing burial depths were less.

All samples (ignoring the Neogene sample) were at sufficient temperatures (>~110 °C) in the Late Permian to reset their fission-track ages to zero. Therefore all were buried at least about 2–4 km. This suggest that at least 2–4 km of Permian strata formerly buried the stratigraphically shallowest sample. Only about 1 km of such higher section is preserved in our sampling area, but about 2.2 km is preserved near Yingan (e.g., Carroll et al., this volume; Fig. 8A) and an even thicker overburden, subsequently partly removed by erosion in the Late Permian, is permissible.

All samples suggest slow cooling through middle Mesozoic to middle Cenozoic time (Fig. 9). In Cenozoic time, samples cooled from temperatures of ~50 °C to surface temperatures, indicating ~2 km of unroofing. The modeling permits this cooling to have occurred at any time within about the past 50 m.y. and cannot provide better definitions. Data from areas to the east and west suggest that Cenozoic folding and thrusting may have started ca. 21–24 Ma, and this is probably the best inference for the timing of major shortening in the Aksu area (Sobel and Dumitru, 1997; Yin et al., 1998).

The Kalpin fold and thrust belt exhibits a major angular unconformity between Permian and older strata and Neogene and younger foreland basin deposits. The fission-track data indicate that this major erosion initiated in middle Permian time, and about 5 km of erosion is indicated for the Sinian (Precambrian) age rocks in the Kalpin area. The Neogene fission-track sample yields an age essentially identical with the ca. 214 Ma age from the Sinian to Permian section. This suggests that the Neogene sample had a local source, consistent with the detrital mineralogy of the Neogene rocks in the area (Graham et al., 1993).

Mesozoic strata are entirely absent in the Kalpin region and stratigraphic relations suggest that the Kalpin area was relatively high throughout Mesozoic time (e.g., Sobel, 1999a; Carroll et al., this volume). The fission-track data are consistent with significant middle Permian deformation and exhumation followed by subsequent relative quiescence (slow erosion) during Mesozoic time.

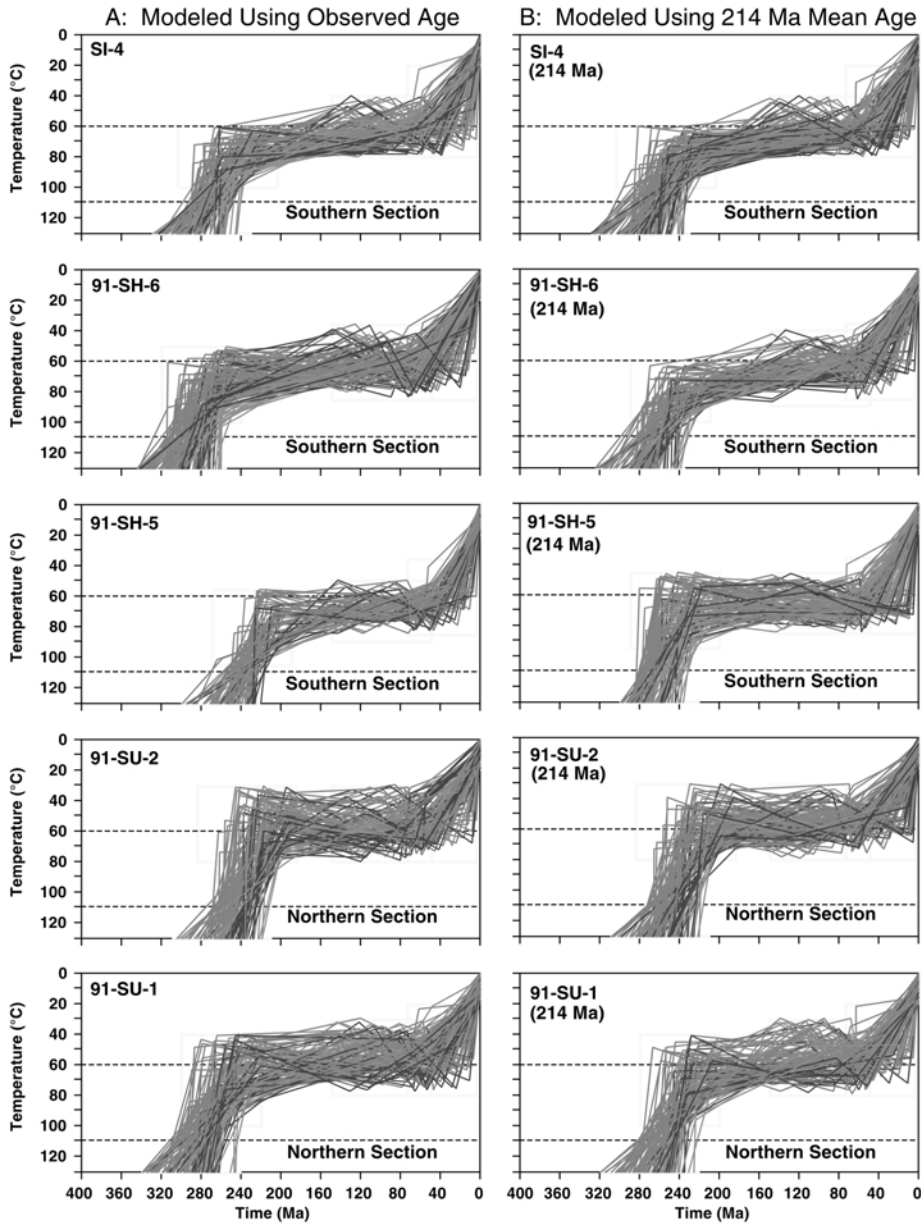

Figure 9. Modeling results from Aksu samples. Modeling was run twice, using individual observed ages (A): and using 214 Ma weighted mean age (B). 214 Ma runs probably yield most accurate results. For all samples, note strong cooling below 100 °C ca. 250 ± 10 Ma, indicating major exhumation at that time. Models then indicate relative quiescence until late Cenozoic time, when further cooling occurred. Specific time of late Cenozoic cooling is not well determined by data, because Cenozoic burial depths were shallower than main sensitivity range of fission-track system. As in Figure 6D, note that parts of histories hotter than ~110 °C are not significant.

A less likely alternate interpretation of the fission-track data from the Aksu area is that they reflect major heating of the section by Early Permian volcanism. As discussed by Carroll et al. (this volume), two series of basaltic lavas crop out in the sampling areas and underlie a large area of the northwest Tarim basin. In outcrop, each series totals ~150–200 m in thickness and consists of multiple thin flows. It appears unlikely that these volcanics reset the fission-track ages, because (1) the total flow thicknesses (and thus heat content) are quite small relative to the ~7.5 km total thickness of the section; (2) the individual flows are thin and so would rapidly lose virtually all of their heat to the atmosphere; and (3) available vitrinite reflectance data indicate minimal heating in the area (Graham et al., 1990). However, this regional volcanism suggests that geothermal gradients in the area may have been higher in the Permian than the 22 °C/km we have assumed for other areas. We have therefore used assumed gradients between 22 and 50 °C/km for the Permian paleotemperature to depth conversions for Aksu discussed here.

Kuqa River transect, southern Tian Shan thrust belt

Yin et al. (1998) described the Baicheng-Kuqa thrust system as an ~400-km-long segment of the southern Tian Shan thrust system. The segment is characterized by a major south-vergent thrust, the Kuqa thrust. The thrust is exposed in the

areas more than about 20 km east of the Kuqa River, where it juxtaposes Carboniferous strata over Neogene–Quaternary sediments (Fig. 10). To the west closer to the Kuqa River, it dies out into a broad anticline as the magnitude of slip decreases. Thrusting and folding in the Kuqa River area is complex; several north-vergent folds and thrusts are exposed on the forelimb of the south-vergent anticline. In general, the Cretaceous and younger strata are tightly folded, whereas folds in Permian to Jurassic strata are more open (Yin et al., 1998).

We collected seven samples in this area before Yin et al. (1998) completed their structural work. In Figure 10 we have projected these samples onto their map and cross section. The results from Kuqa are fairly complex, probably because several different fault slices were sampled (Fig. 10). The four stratigraphically oldest samples yielded similar data; single-grain ages and sample ages cluster ca. 85 Ma and broad track length distributions are indicative of multistage cooling histories (Fig. 11). Modeling shows that the data are consistent with a two-stage cooling history, the first cooling starting from total annealing temperatures (≥110–125 °C) with cooling through ~100 °C ca. 110 ± 20 Ma, followed by cooling from partial annealing temperatures of 60–90 °C in the late Cenozoic (after ca. 30 Ma) (Fig. 12B). The consistency of data over a 7 km map distance suggests that the ca. 110 Ma cooling was a strong unroofing event. Strong unroofing ca. 110 Ma is consistent with a major unconformity overlain by conglomerate in the Tarim basin section at about that time, as discussed in the following. Generally similar age cooling occurred along parts of the

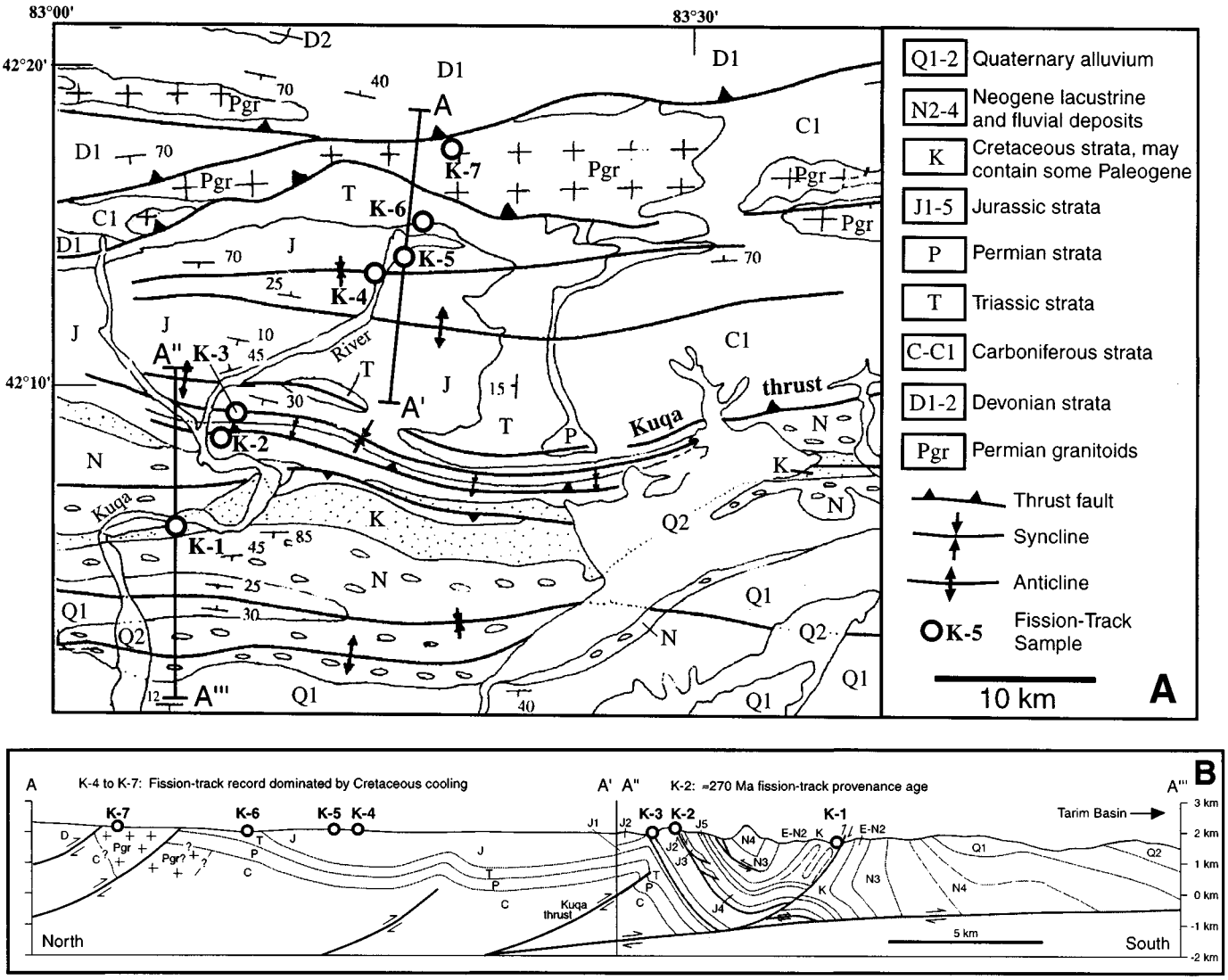

Figure 10. A: Geologic map of southern flank of Tian Shan north of town of Kuqa, with fission-track sample localities. Map reproduced directly from Yin et al. (1998), who compiled it primarily from mapping of Xinjiang Bureau of Geology and Mineral Resources (1966). B: Cross section A–A‴. Southern part of section is directly from Yin et al. (1998), based on their new mapping in that area. Northern part of section is our tentative interpretation from map in A.

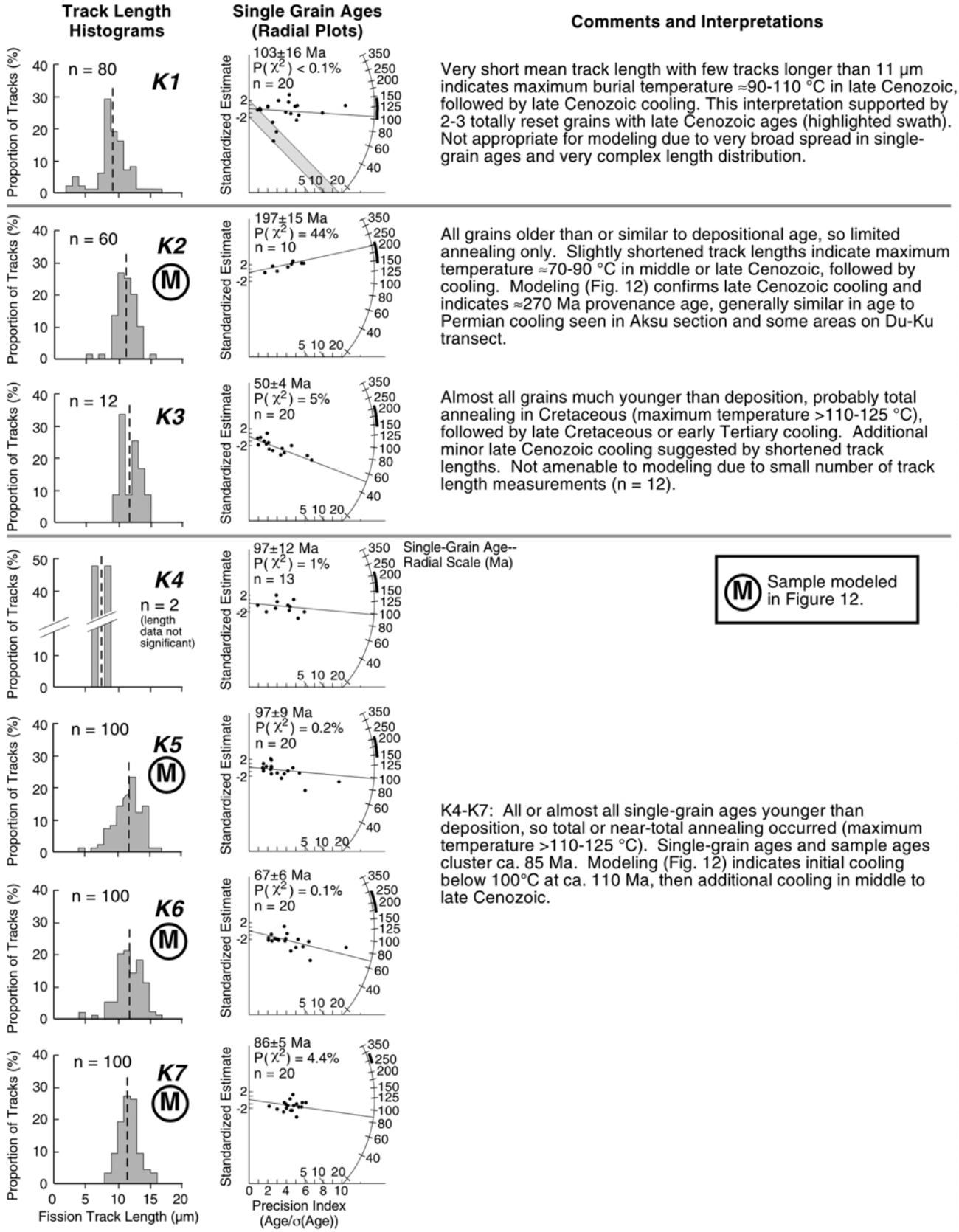

Figure 11. Fission-track data and interpretations from Kuqa samples. Four of these samples (M) are modeled in Figure 12.

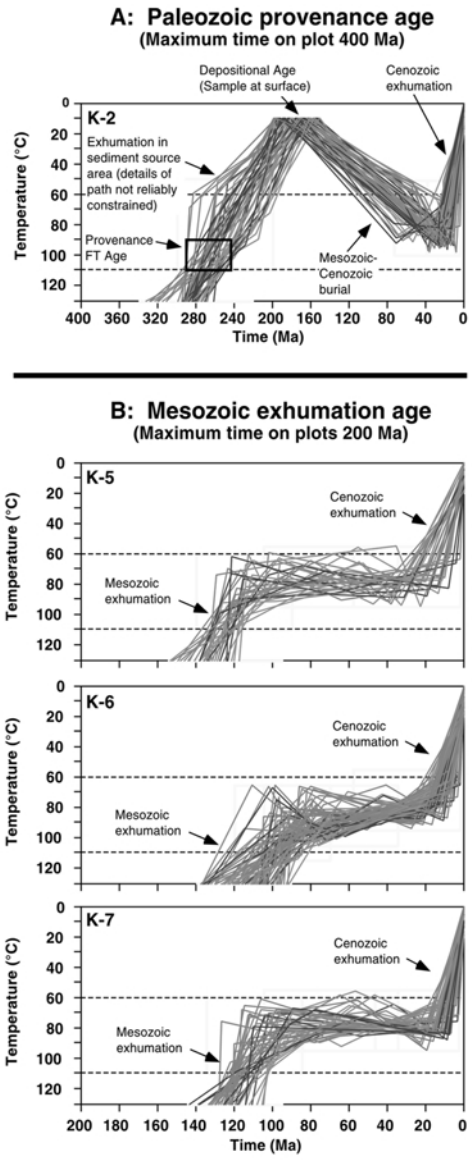

Figure 12. Modeling results for four Kuqa samples. Northernmost three samples (K-5, K-6, K-7) indicate major cooling below 100 °C ca. 110 ± 20 Ma. Range in ages may be real and could represent somewhat different times of exhumation through 100 °C isotherm at different sample sites, which are ~7 km apart, or may reflect errors in data. Sample K-2, with Jurassic depositional age, records cooling below 100 °C in sediment provenance areas ca. 270 Ma. All samples also record late Cenozoic cooling, but modeling cannot constrain specific time. Parts of histories hotter than ~110 °C are not significant.

Dushanzi-Kuqa corridor, and provide additional evidence for a significant late Mesozoic cooling episode.

The stratigraphically youngest sample (K1) is from an area of complex Cenozoic deformation (Fig. 10). This sample has a very short mean track length of 9.5 μm with few tracks longer than 11 μm. This indicates exposure to burial temperatures of 90–110 °C (burial depth on the order of 4 km) in the late Cenozoic, after almost all of the tracks had formed, followed by unroofing to expose the sample at the surface (Fig. 11). Much of the overburden was probably tectonic burial during Cenozoic folding and thrusting, because the Cretaceous to Neogene stratigraphic thicknesses are too thin to bury the sample so deeply (Zhang, 1981).

Samples K2 and K3 are from Jurassic strata exposed on the limb of a syncline, where K3 is situated about 1 km stratigraphically downsection from K2. Modeling shows that K2 records cooling below ~100 °C ca. 260 Ma, much older than the depositional age. This age reflects cooling ages in the source areas for the Jurassic sediments and is similar to the latest Paleozoic cooling episode seen at Aksu and along parts of the Dushanzi-Kuqa corridor. Only sparse track length data could be collected for sample K3. Modeling (not shown) suggests cooling in early Tertiary time, but given the sparse length data this result is not very robust. Both samples record additional cooling in the late Cenozoic, from temperatures of ~80–90 °C, indicating about 3 km of unroofing.

The fission-track data unfortunately contribute little to precisely dating Cenozoic thrusting and exhumation history of the Kuqa area, because the samples have undergone too little Cenozoic exhumation for the fission-track system. Yin et al. (1998) suggested that initial significant thrusting may have begun at 24–21 Ma, based on the time of a major facies change from lacustrine to braided-fluvial sequences in the Tarim basin section. A generally similar timing for initiation of Cenozoic shortening has been reported from other areas around the Tarim and Junggar basins (Hendrix et al., 1994; Sobel and Dumitru, 1997).

The major ca. 110 Ma unroofing event recorded by the four northernmost samples is more interesting. A significant mid-Cretaceous unconformity is present in the north Tarim, south Junggar, and Turpan basins (Hendrix et al., 1992). Age control on the nonmarine Cretaceous strata in western China is problematic, but it appears that strata with ages from ca. 120 Ma to ca. 98 Ma are missing along the unconformity. The fission-track modeling indicates a minimum of about 1.5 km of unroofing at this time. This is apparently a major widespread event involving major erosion within parts of the Tian Shan core and adjacent basins.

Dushanzi-Kuqa corridor

The Dushanzi-Kuqa Highway (Du-Ku) crosses the core of the Tian Shan from Kuqa on the south to Dushanzi on the north (Fig. 3). Zhou et al. (this volume) summarize the geology along the road corridor, with emphasis on the Paleozoic and earlier history. Very little is known about the Mesozoic and Cenozoic deformational history of the area. Use of the road has been highly restricted and the time available for us to sample and make field observations was severely limited.

Figures 3, 13, and 14 and Table 1 summarize fission-track data from this area, and the fission-track samples are also indicated on the cross-sectional road log of Zhou et al. (this volume). The approach used to interpret these data is somewhat different from that used in the other sampling areas. In the other

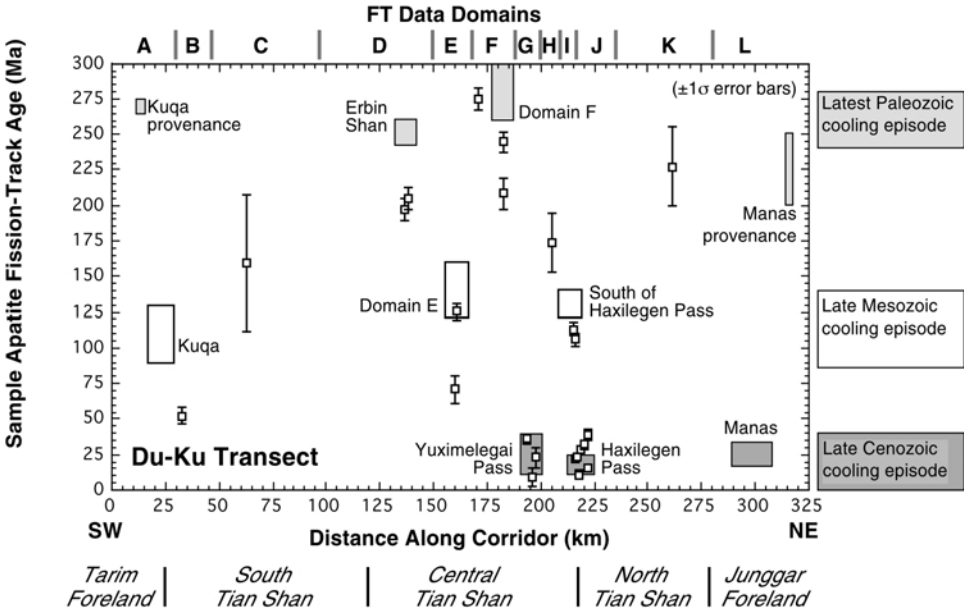

Figure 13. Plot of observed fission-track ages (points) versus location along Du-Ku corridor (Fig. 3). Ages are not shown for Kuqa and Manas (see Figs. 6 and 11). Plot shows domains A to L with consistent fission-track data discussed in text. Boxes indicate main times of cooling below ~100 °C indicated by modeling.

areas, suites of samples could be collected from individual areas with at least some degree of structural control, such as sample position within partially intact stratigraphic successions. An integrated interpretation could then be derived for the suite of samples. Along the Du-Ku transect, structural control is essentially unavailable and generally only a few samples were analyzed from each area. In this case, the track length and age data are then modeled to determine the range of permitted time-temperature histories. Broader geologic issues may then be addressed by interpreting the variations in time-temperature histories across the range.

The data from the transect can be tentatively divided into 12 domains, A–L, that yield reasonably consistent histories. Domains A and L are the Kuqa and Manas sections discussed previously, where the dominant times of cooling recorded by the fission-track system were ca. 110 and 25 Ma, respectively.

Domains B and C comprise two poor quality samples of lower Paleozoic sedimentary strata (Figs. 3, 13, and 14). These sample yielded ages of 52 ± 6 Ma and 159 ± 48 Ma. Useful track length data could not be collected and a detailed interpretation of these samples is not possible. One important conclusion is that late Cenozoic unroofing of these samples has been limited, <~5 km, because the samples have not been hot enough to totally reset fission-track ages to zero during late Cenozoic time.

Domain D comprises two samples in the Erbin Shan of the central Tian Shan block that have concordant ages of 197 ± 8 and 205 ± 8 Ma. Sample DK-55 is from a Devonian? granite (378 U-Pb age, Hu et al., 1986; Zhou et al., this volume) and DK-61 is from an overlying Lower Carboniferous conglomerate. DK-55 yielded a potassium feldspar $^{40}Ar/^{39}Ar$ standard step-heating age spectra that rises slowly from 252 to 277 Ma (Zhou et al., this volume). Modeling of the fission-track data from these samples indicates major cooling below 100 °C ca. 250 Ma, followed by slow cooling until a final episode of cooling some time in the late Cenozoic (Fig. 15A). The early cooling ca. 250 Ma is essentially concordant with the cooling indicated by the $^{40}Ar/^{39}Ar$ data. This indicates strong cooling, probably from temperatures hotter than ~300–350 °C to cooler than ~80 °C at that time. This is very similar in timing to the latest Paleozoic cooling episode recorded at Aksu.

Domain E comprises six samples of metamorphic and granitic rocks (Fig. 3, 13, and 14). The ages of four of these samples, which were collected within about 2 km of each other, range from 106 to 135 Ma. The remaining two samples were of very poor quality and were not interpreted. Sample J5 yielded a biotite $^{40}Ar/^{39}Ar$ plateau age of 286.1 ± 2.6 Ma (Zhou et al., this volume), suggesting it cooled below ~350 °C in late Paleozoic time. Fission-track modeling indicates that these samples cooled below ~100 °C between ca. 160 and 120 Ma (Fig. 15B). Three of the samples exhibit relatively slow late Mesozoic cooling rates and the spread in cooling times may reflect the fact that different samples cooled through the ~100 °C isotherm at different times during a protracted period of relatively slow erosion in the area. This timing of cooling is generally similar to the late Mesozoic cooling recorded at Kuqa.

Domain F comprises three samples of igneous rocks with ages of 208 to 275 Ma. Samples DK-43 and DK-44 were collected about 1 km apart and yield compatible modeled histories (Fig. 15A) if DK-43 is assumed to have resided 0.5–1.0 km higher in the crust in late Paleozoic time. DK-43 cooled below 100 °C ca. 280 Ma, reaching ~65 °C thereafter. DK-44 cooled below 100 °C later, ca. 260 Ma, and then reached ~80 °C. These contrasting histories are compatible with slow cooling in late Paleozoic time. Sample DK-45 cooled below 100 °C ca. 300 Ma. All three samples then experienced further cooling in late Cenozoic time.

Domain G comprises three samples from near Yuximelegai Pass with ages of 9.1, 22.7, and 35.7 Ma. These young ages

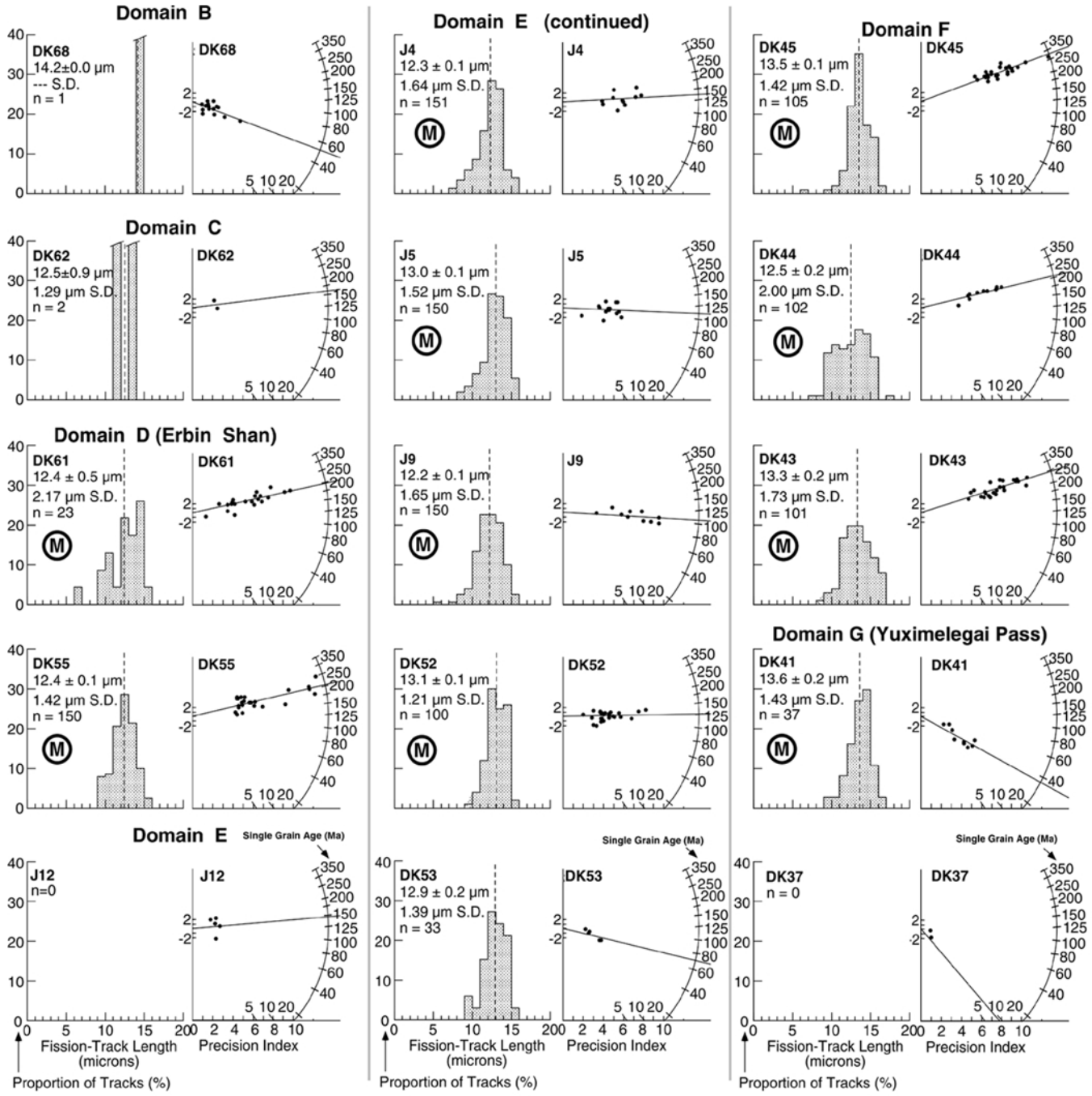

Figure 14. Fission-track data from samples collected along Dushanzi-Kuqa corridor. Samples indicated with M are modeled in Figure 15.

suggest that this area is a site of significantly more Cenozoic unroofing than areas to the south. Only DK-41 yielded sufficient track length data to allow modeling. This sample indicates a complex cooling history with major cooling below ~100 °C at about 40 Ma, and additional cooling in the past 15 m.y. (Fig. 15C). The other two samples that could not be modeled have younger sample ages and corroborate major cooling since ca. 25 Ma.

Domain H comprises a single poor sample with an age of 174 Ma. This sample was not interpreted. It is clear that it has been exhumed no more than about 5 km in Cenozoic time.

Domain I comprises two samples with ages of 106 and 113 Ma. These samples are just south across a possible major Cenozoic fault system from much younger samples in domain J. Modeling indicates cooling below 100 °C ca. 140–120 Ma (Fig. 15B), generally similar to the late Mesozoic cooling seen in Domain E.

Domain J comprises eight samples near Haxilegen Pass with ages of 11–39 Ma (Figs. 3, 13, and 14). Five of these samples yielded sufficient track length data to permit modeling. Sample DK-27 yields the youngest time of cooling, with cool-

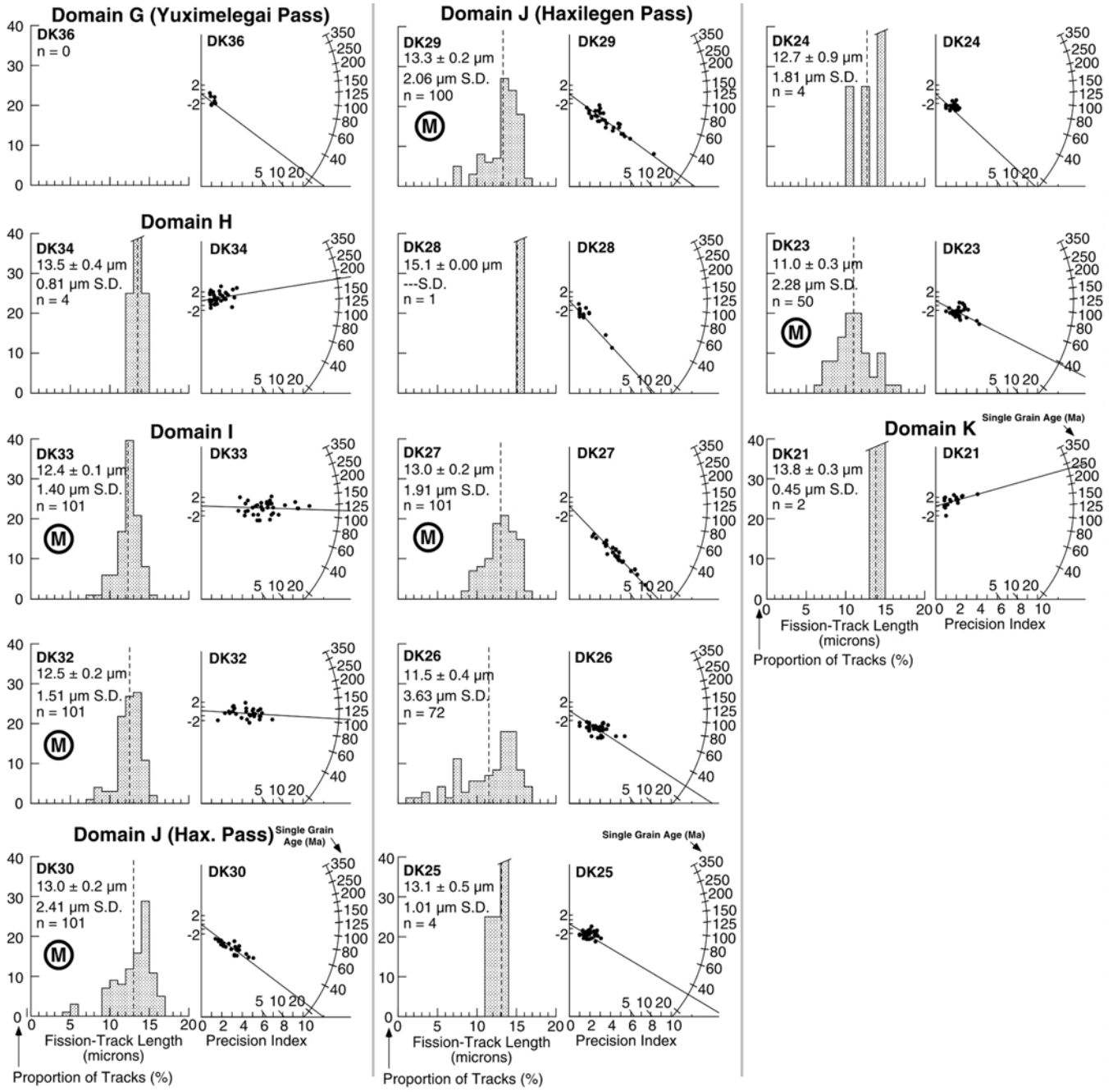

Figure 14. (*continued*)

ing below 100 °C ca. 11 Ma. The other four samples also underwent strong cooling within the past 20 m.y. Several of the samples record earlier cooling sometime between 70 and 40 Ma (Fig. 15C).

Haxilegen Pass is the approximate location of the north Tian Shan fault system, which forms the current boundary between the north Tian Shan and central Tian Shan blocks (Fig. 3) (Zhou et al., this volume). Essential no field data have been published on this fault system. Several recent regional maps (e.g., Ma, 1986; Hendrix et al., 1992; Yin et al., 1998) seem to show it as a major right-lateral strike-slip fault system (with various names), although it was not identified in the pioneering Landsat interpretation of Tapponnier and Molnar (1979). Assuming that such interpretations are generally correct, it is likely that a complex network of Cenozoic faults passes near Haxilegen Pass and that the fission-track samples are from various structural blocks. Thus, the fission-track data confirm that the fault system has been a site of active deformation and exhumation during the Cenozoic. Uplift and exhumation along major strike-slip fault systems is common and may be ascribed to either of two mechanisms. It

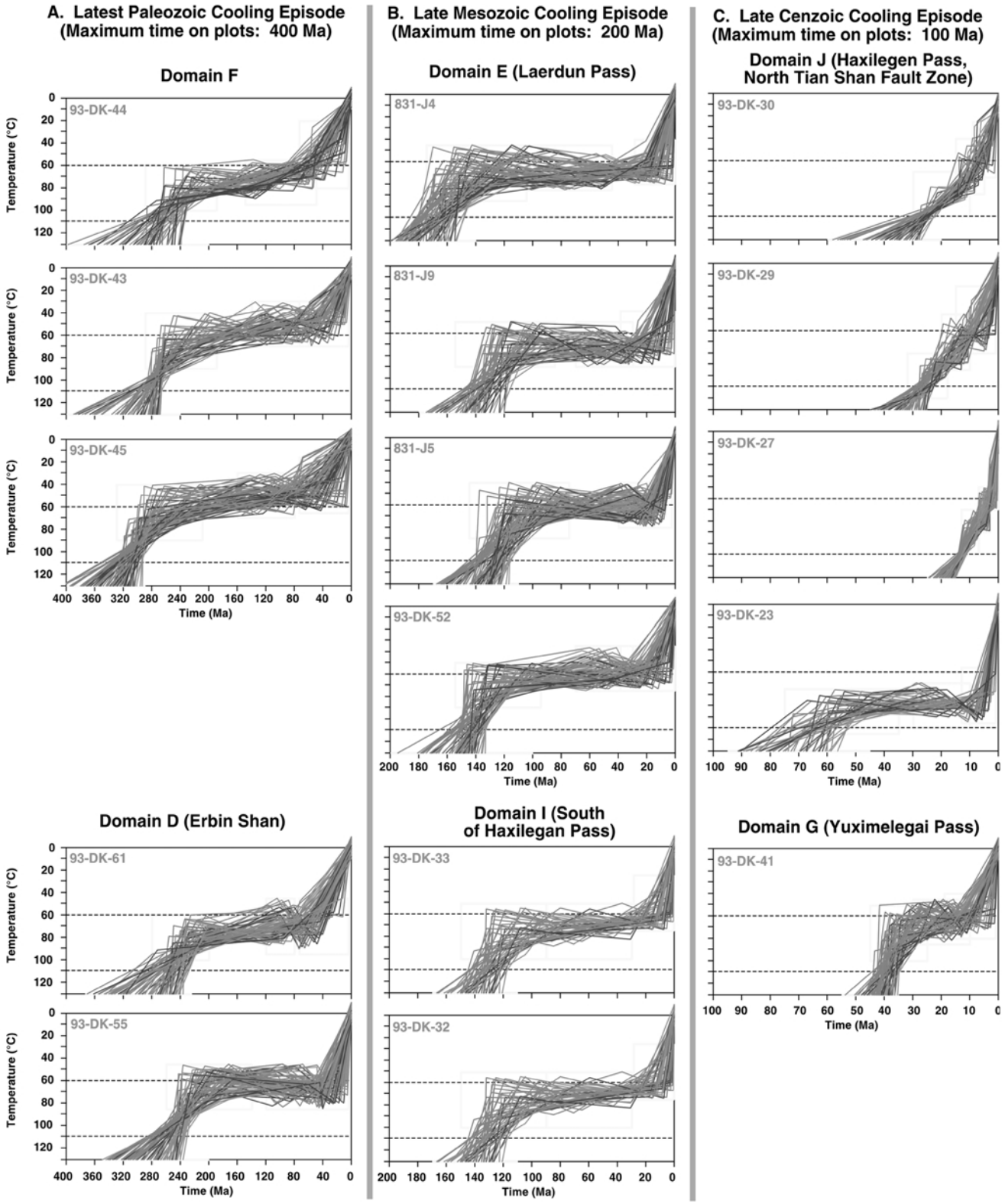

Figure 15. Modeling of samples from Dushanzi-Kuqa corridor. Various areas (domains) that record similar times of cooling are grouped together. See text for discussion. Note that model histories from Aksu (Fig. 9) and Kuqa sample K-2 (Fig. 12) are generally similar to latest Paleozoic histories shown here, and histories from Kuqa samples K-5 to K-7 are generally similar to late Mesozoic histories shown here. Parts of histories hotter than ~110 °C are not significant.

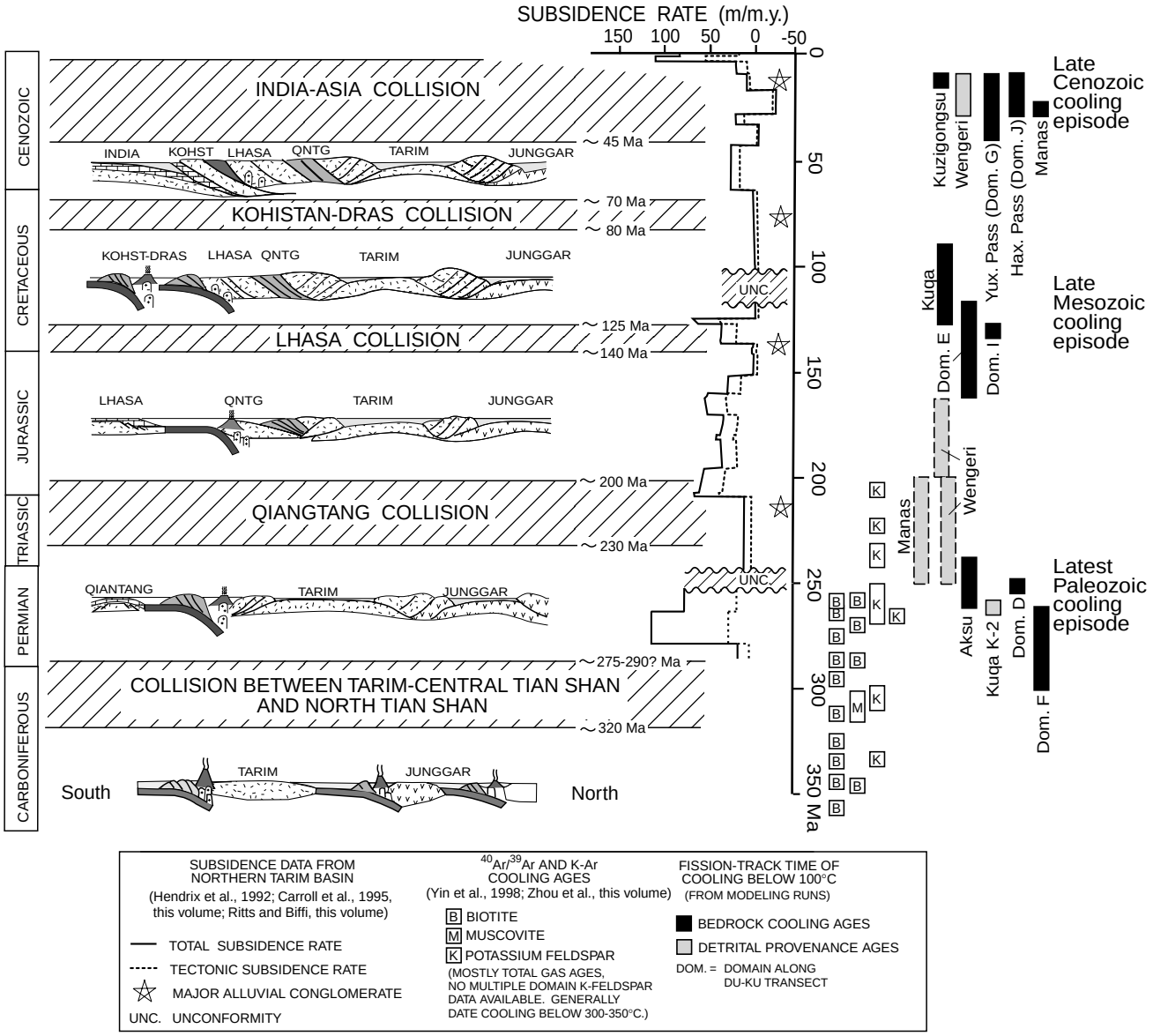

Figure 16. Summary diagram of indicators of timing of deformation in Chinese Tian Shan. Subsidence history in northern Tarim basin shows rapid subsidence during India-Asia collision and earlier periods of accelerated subsidence that appear to correlate with late Paleozoic and Mesozoic collisions at southern margin of Asia. Almost all available K-Ar and $^{40}Ar/^{39}Ar$ cooling ages are older than 250 Ma. Times of cooling below 100 °C appear to cluster in late Cenozoic, late Mesozoic, and latest Paleozoic time. See Figure 2 for locations. Cross sections modified from Watson et al. (1987). QNTG.—Qiantang.

may occur due to a component of regional transpression across the fault system, or may occur due to space problems along bends and steps in the fault system (e.g., Dumitru, 1991; Bürgmann et al., 1994). Predominately dip-slip secondary faults that root into the main strike-slip system are common in such settings.

Domain K comprises a single poor sample with an age of 227 Ma. This sample was not interpreted.

Domain L comprises the Manas section of the Junggar basin sequence discussed previously, where the fission-track data record major exhumation ca. 25 Ma (Fig. 6). The Manas section is not along the Du-Ku road, but is about 75 km to the east.

DISCUSSION AND CONCLUSIONS

Previous studies have indicated that the Tian Shan has undergone multiple episodes of deformation since initial suturing of the Tarim, central Tian Shan, and north Tian Shan blocks in Paleozoic time. The highly heterogeneous fission-track cooling record is certainly consistent with this. Figures 2 and 16 compile the times of cooling recorded by the fission-track system in the various areas and compare them with what is known about the timing of various collisional events on the southern margin of Asia. The available fission-track data cluster mainly

in three time intervals, defining latest Paleozoic, late Mesozoic, and late Cenozoic cooling episodes (Fig. 16).

Latest Paleozoic cooling episode

Latest Paleozoic cooling is indicated at Aksu and in domains D and F along the Du-Ku corridor. Available $^{40}Ar/^{39}Ar$ cooling ages from the Tian Shan also tend to cluster at this time; there are very few younger ages (Fig. 16). At Aksu, additional timing constraints are provided by the age of the youngest essentially conformable nonmarine clastic strata preserved in the section, which must predate the time of exhumation. These units have generally been assigned an Upper Permian age, but are barren of fossils; a Lower Permian age is also possible (e.g., Carroll et al., this volume). In domain D in the Erbin Shan, potassium feldspar $^{40}Ar/^{39}Ar$ and apatite fission-track data indicate that sample DK-55 cooled from temperatures >300–350 °C to <80 °C ca. 270–250 Ma.

The collision of the Tarim–central Tian Shan composite block with the north Tian Shan apparently occurred in Late Carboniferous–Early Permian time. However, the data constraining this timing are very limited and it is plausible that the collision was diachronous east-west along the length of the Tian Shan (as was the India-Asia collision), that deformation within the Tian Shan was focused at different places at different times, and that exhumation continued for a period after the actual collision ended. The significant number of middle- to Late Permian $^{40}Ar/^{39}Ar$ cooling ages in the range (Fig. 16) suggests that strong deformation continued into Late Permian time. This is also consistent with interpretations from the Junggar basin, where Carroll et al. (1995) inferred a foreland basin setting linked to shortening and uplift in the Tian Shan, based on facies and subsidence patterns. Thus we tentatively ascribe the latest Paleozoic cooling episode to deformation and exhumation induced by the collision, but remain cautious because much of the cooling appears to significantly postdate the currently favored estimates for the age range for the collision.

Late Mesozoic cooling episode

Late Mesozoic cooling within the Tian Shan is recorded by fission-track data from Kuqa, as well as domains E and I within the Tian Shan core (Figs. 2, 3, and 16). This time of cooling coincides broadly with a significant unconformity within the stratigraphic section of the northern Tarim basin (Zhang, 1981) as well as a period of coarse conglomeratic sedimentation within the north Tarim and south Junggar foreland depocenters inferred to reflect episodic deformation and physiographic rejuvenation of the range (Hendrix et al., 1992). The general age of cooling in these areas is also consistent with deformation in the southeastern Junggar basin, where subsurface data show that Jurassic strata are cut by reverse faults and overlapped by undeformed Cretaceous strata (Li and Jiang, 1987). Deformation of this age is reasonably widespread across western China and may reflect structural reactivation of the Tian Shan by the collision of the Lhasa block onto the south Asian continental margin during latest Jurassic–earliest Cretaceous time (e.g., Hendrix et al. 1992). The Lhasa block is located in the southern portion of the Tibetan Plateau, and extends from the Banggong suture south to the Indus suture (Fig. 1). Precollision flysch sequences associated with the Banggong suture are entirely Jurassic in age (Girardeau et al., 1984; see also Matte et al., 1996). These, along with Tithonian radiolaria preserved in deep-sea cherts that crop out in the suture, indicate that closing of the suture was some time during or after the latest Tithonian, perhaps continuing into the earliest Cretaceous (Smith, 1988). Uppermost Jurassic–lowermost Cretaceous nonmarine to shallow-marine sediments, which overlap the obducted Donqiao-Gyanco ophiolite associated with the Banggong suture, provide an upper bound for the age of accretion of the Lhasa block (Girardeau et al., 1984).

Uplift in the Mesozoic in the Tian Shan, however, was clearly heterogeneous across the core of the range, as indicated by fission-track records for late Mesozoic cooling in some areas, the preservation of records of latest Paleozoic cooling in other areas, and the deposition of Jurassic intermontane basin sections in still others areas (Figs. 2, 3, 4, and 16). The late Mesozoic Tian Shan was likely characterized by several uplifted ranges and intervening intermontane basins; a generally east-west trend in structural grain is indicated by the preserved trends of the intermontane basins. Thus the Mesozoic physiography of the Tian Shan somewhat resembled that of the modern Tian Shan, and Cenozoic reactivation of Mesozoic structural trends probably helped shape the modern range.

In addition to the Lhasa block collision, Hendrix et al. (1992) concluded that collision of the Qiangtang block and Kohistan-Dras arc system (Fig. 1) with the southern margin of Asia deformed the Chinese Tian Shan and resulted in pulses of coarse clastic sedimentation in the southern Junggar and northern Tarim basins. The available fission-track data do not provide evidence for these Mesozoic tectonic events, except perhaps the Qiangtang collision in provenance ages at Wenguri and Manas (Fig. 16). This suggests that the deformation they caused within the Tian Shan was too minor to be recorded by the fission-track system, or that any such deformation affected other unsampled areas of the range. In the Altyn Tagh, on the southeast side of the Tarim basin, Sobel et al. (this volume) document Early to Middle Jurassic cooling inferred to reflect the Qiangtang collision (Fig. 2). That region is much closer to the collision zone, so it is not surprising that a record of tectonism may be preserved there but not in the Tian Shan. Cooling that might be linked to the Lhasa block collision is not apparent in the transect of Sobel et al. (this volume), but may be recorded at a second transect farther east in the Altyn Tagh (Delville et al., this volume).

This preceding discussion assumes that collisions at Asia's southern margin were the tectonic drivers for Mesozoic deformation in the Tian Shan. However, there is no direct evidence for this in the cooling and sedimentation records. It is alternately possible that poorly understood interactions at other Asian margins

drove Mesozoic deformation in the range, such as the Mesozoic closure of the Mongol-Okhosk seaway (e.g., Halim et al., 1998).

Late Cenozoic cooling episode

One of the most significant conclusions from the current data set is that much of the Chinese Tian Shan has undergone only modest total unroofing during Cenozoic time, despite the great relief and strong seismicity in the modern-day range. Most sampling areas underwent no more than about 3 km of late Cenozoic unroofing. The areas on the margins of the Tarim and Junggar basins that have undergone greater late Cenozoic unroofing include the base of the Kuzigongsu section (~4–5 km), the sediment source areas for the Miocene Wenguri samples (>5 km), sample K-1 at Kuqa (4–5km), and the base of the section at Manas (4–5 km) (Fig. 2). These Tarim and Junggar data may be somewhat biased toward areas of greatest unroofing because especially thick, intact sections were targeted for sampling. In addition, at least some of these areas were tectonically buried by thrusting and consequent thickening in late Cenozoic time, so part of the total unroofing reflects removal of this extra tectonic burial. Within the interior of the Chinese Tian Shan, only the Yuximelegai Pass and Haxilegen Pass areas reveal more than 5 km of late Cenozoic unroofing. Thus, these data lead to a general picture of late Cenozoic deformation of the Chinese Tian Shan where strong uplift, seismicity, and deformation are occurring, but the amount of erosion from the range has been limited (cf. Yin et al., 1998).

The available fission-track data have recorded major Cenozoic unroofing within the interior of the range in only two areas, near Yuximelegai and Haxilegen Passes (Fig. 3). Haxilegen Pass apparently is astride the north Tian Shan fault system (e.g., Ma, 1986; Zhou et al., this volume). The fission-track data demonstrate that this fault system has been strongly reactivated in Cenozoic time. General regional relations suggest that this may be a west-northwest–trending, right-lateral strike-slip or transpressional fault. As such, it may be an important member of the system of major strike-slip faults that is helping to accommodate deformation in central Asia induced by the India-Asia collision (e.g., Tapponnier and Molnar, 1979). However, the fission-track data cannot specifically document strike-slip motions on the system and so cannot rule out a predominately dip-slip sense of offset at Haxilegen Pass.

ACKNOWLEDGMENTS

This research was supported by the Stanford–China Geosciences Industrial Affiliates and the Stanford McGee and Shell Funds. We are grateful to Wang Baoyu, Xiao Xuchang, Fu Derong, Jia Mingming, Liu Xun, Wang Zuoxun, Don Ying, the Chinese Academy of Geological Sciences, and the Xinjiang Bureau of Geology and Mineral Resources for collaboration in the field. We thank Tina Bush-Rester and Dean Miller for help with sample preparation and drafting, David Coyle and Kerry Gallagher for providing software, and Nicholas Arnaud and Ann Blythe for reviewing the manuscript. The Texas A&M University Nuclear Science Center and University of Oregon Radiation Center provided sample irradiations.

REFERENCES CITED

Academy of Geological Sciences of China, 1975, Geological map of Asia: Beijing, Geologic Publishing House, scale 1:5 000 000.

Allen, M.B., Windley, B.F., and Zhang, C., 1992, Paleozoic collisional tectonics and magmatism of the Chinese Tien Shan, central Asia: Tectonophysics, v. 220, p. 89–115.

Allen, M.B., Vincent, S.J., and Wheeler, P.J., 1999, Late Cenozoic tectonics of the Kepingtage thrust zone: Interactions of the Tien Shan and Tarim basin, northwest China: Tectonics, v. 18, p. 639–654.

Arnaud, N.O., 1992, Apport de la thermochronologie $^{40}Ar/^{39}Ar$ sur feldspath potassique à la connaissance de la tectonique Cenozoique d'Asie [Ph.D. thesis]: Clermont-Ferrand, France, Université du Clermont-Ferrand 2, 161 p.

Arnaud, N., Brunel, M., Cantagrel, J.M., and Tapponnier, P., 1993, High cooling and denudation rates at Kongur Shan (Xinjiang, China) revealed by $^{40}Ar/^{39}Ar$ K-feldspar thermochronology: Tectonics, v. 12, p. 1335–1346.

Avouac, J.P., Tapponnier, P., Bai, M., You, H., and Wang, G., 1993, Active thrusting and folding along the northern Tien Shan and late Cenozoic rotation of the Tarim relative to Dzungaria and Kazakhstan: Journal of Geophysical Research, v. 98, p. 6755–6804.

Brunel, M., Arnaud, N., Tapponnier, P., Pan, Y.S., and Wang, Y., 1994, Kongur Shan normal fault: Type example of mountain building assisted by extension (Karakoram fault, eastern Pamir): Geology, v. 22, p. 707–710.

Burbank, D.W., and Bullen, M.E., 1999, Late Cenozoic rates of rock and surface uplift in the Central Kyrgyz Range, Northern Tien Shan [abs.]: Eos (Transactions, American Geophysical Union), v. 80, p. F1035.

Bürgmann, R., Arrowsmith, R., Dumitru, T., and McLaughlin, R., 1994, Rise and fall of the southern Santa Cruz Mountains, California, from fission-tracks, geomorphology, and geodesy: Journal of Geophysical Research, v. 99, p. 20181–20202.

Burtman, V.S., Skobelev, S.F., and Molnar, P., 1996, Late Cenozoic slip on the Talas-Ferghana fault, the Tien Shan, central Asia: Geological Society of America Bulletin, v. 108, p. 1004–1021.

Carroll, A.R., Liang, Y., Graham, S.A., Xiao, X., Hendrix, M.S., Chu, J., and McKnight, C.L., 1990, Junggar basin, northwest China: Trapped late Paleozoic ocean: Tectonophysics, v. 181, p. 1–14.

Carroll, A.R., Graham, S.A., Hendrix, M.S., Ying, X., and Zhou, D., 1995, Late Paleozoic tectonic amalgamation of northwestern China: Sedimentary record of the northern Tarim, northwestern Turpan, and southern Junggar basins: Geological Society of America Bulletin, v. 107, p. 571–594.

Cerveny, P.F., Naeser, N.D., Zeitler, P.K., Naeser, C.W., and Johnson, N.M., 1988, History of uplift and relief of the Himalaya during the past 18 million years: Evidence from fission-track ages of detrital zircons from sandstones of the Siwalik Group, *in* Kleinspehn, K.L., and Paola, C., eds., New perspectives in basin analysis: New York, Springer-Verlag, p. 43–61.

Chen, Z., Wu, N., Zhang, D., Hu, J., Huang, H., Shen, G., Wu, G., Tang, H., and Hu, Y., 1985, Geological map of Xinjiang Uygur Autonomous Region, China: Beijing, Geological Publishing House, scale 1:2 000 000.

Corrigan, J.D., 1991, Inversion of apatite fission-track data for thermal history information: Journal of Geophysical Research, v. 96, p. 10347–10360.

Corrigan, J.D., 1993, Apatite fission-track analysis of Oligocene strata in south Texas, U.S.A.: Testing annealing models: Chemical Geology, v. 104, p. 227–249.

Dumitru, T.A., 1988, Subnormal geothermal gradients in the Great Valley forearc basin, California, during Franciscan subduction: A fission-track study: Tectonics, v. 7, p. 1201–1221.

Dumitru, T.A., 1991, Major Quaternary uplift along the northernmost San Andreas fault, King Range, northwestern California: Geology, v. 19, p. 526–529.

Dumitru, T.A., 1993, A new computer-automated microscope stage system for fission-track analysis: Nuclear Tracks and Radiation Measurements, v. 21, p. 575–580.

Dumitru, T.A., 2000, Fission-track geochronology, *in* Knoller, J.S., et al., eds., Quaternary geochronology: Methods and applications: American Geophysical Union Reference Shelf, v. 4, p. 131–156.

Dumitru, T.A., Miller, E.L., O'Sullivan, P.B., Amato, J.M., Hannula, K.A., Calvert, A.C., and Gans, P.B., 1995, Cretaceous to recent extension in the Bering Strait region, Alaska: Tectonics, v. 14, p. 549–563.

Fan, S.F., Zhou, Z.Y., Pan, C.C., Han, L., and Zhu, Y.M., eds., 1990, Paleotemperature and oil and gas of Tarim: Oil and gas geology of Tarim basin: Beijing, Science Press, 77 p.

Galbraith, R.F., 1981, On statistical models for fission-track counts: Mathematical Geology, v. 13, p. 471–478.

Galbraith, R.F., 1990, The radial plot: Graphical display of spread in ages: Nuclear Tracks and Radiation Measurements, v. 17, p. 207–214.

Galbraith, R.F., and Laslett, G.M., 1993, Statistical models for mixed fission-track ages: Nuclear Tracks and Radiation Measurements, v. 21, p. 459–470.

Gallagher, K., 1995, Evolving temperature histories from apatite fission-track data: Earth and Planetary Science Letters, v. 136, p. 421–435.

Gao, Z., Wang, W., Peng, C., and Xiao, B., 1985, The Sinian in Aksu-Wushi area, Xinjiang, China: Urumqi, Xinjiang People's Publishing House, 184 p.

Girardeau, J., Marcoux, J., Allegre, C.J., Bassoullet, J.P., Tang, Y., Xiao, X., Zao, Y., Wang, X., 1984, Tectonic environment and geodynamic significance of the Neo-Cimmerian Donqiao ophiolite, Bangong-Nujiang suture zone, Tibet: Nature, v. 307, p. 27–31.

Gleadow, A.J.W., Duddy, I.R., Green, P.F., and Lovering, J.F., 1986, Confined fission-track lengths in apatite: A diagnostic tool for thermal history analysis: Contributions to Mineralogy and Petrology, v. 94, p. 405–415.

Graham, S.A., Brassell, S., Carroll, A.R., Xiao, X., Demaison, G., McKnight, C.L, Liang, Y., Chu, J., and Hendrix, M.S., 1990, Characteristics of selected petroleum source rocks, Xianjiang Uygur Autonomous Region, northwest China: American Association of Petroleum Geologists Bulletin, v. 74, p. 493–512.

Graham, S.A., Hendrix, M.S., Wang, L., and Carroll, A.R., 1993, Collisional successor basins of western China: Impact of tectonic inheritance on sand composition: Geological Society of America Bulletin, v. 105, p. 323–344.

Graham, S.A., Zhou, D., Chang, E.Z., and Hendrix, M.S., 1994, Origins of intermontane Jurassic strata of the Chinese Tian Shan: Geological Society of America Abstracts with Programs, v. 26, no. 7, p. A464.

Green, P.F., 1981, A new look at statistics in fission-track dating: Nuclear Tracks and Radiation Measurements, v. 5, p. 77–86.

Green, P.F., Duddy, I.R., Gleadow, A.J.W., and Lovering, J.F., 1989a, Apatite fission-track analysis as a paleotemperature indicator for hydrocarbon exploration, *in* Naeser, N.D., and McCulloh, T.H., eds., Thermal history of sedimentary basins: Methods and case histories: New York, Springer-Verlag, p. 181–195.

Green, P.F., Duddy, I.R., Laslett, G.M., Hegarty, K.A., Gleadow, A.J.W., and Lovering, J.F., 1989b, Thermal annealing of fission-tracks in apatite, 4. Quantitative modelling techniques and extension to geological timescales: Chemical Geology, v. 79, p. 155–182.

Halim, N., Kravchinsky, V., Gilder, S., Cogne, J.-P., Alexyutin, M., Sorokin, A., Courtillot, V., and Chen, Y., 1998, A palaeomagnetic study from the Mongol-Okhotsk region: Rotated Early Cretaceous volcanics and remagnetized Mesozoic sediments: Earth and Planetary Science Letters, v. 159, p. 133–145.

Harlan, W.B., Armstrong, R.L., Cox, A.V., Craig, L.E., Smith, A.G., and Smith, D.G., 1990, A geologic time scale 1989: Cambridge, Cambridge University Press, 263 p.

Harrison, T.M., Copeland, P., Kidd, W.S.F., and Yin, A., 1992, Raising Tibet: Science, v. 255, p. 1663–1670.

Hendrix, M.S., 2000, Evolution of Mesozoic sandstone compositions, southern Junggar, northern Tarim, and western Turpan basins, northwest China: A detrital record of the ancestral Tian Shan: Journal of Sedimentary Research, v. 70, p. 520–532.

Hendrix, M.S., Graham, S.A., Carroll, A.R., Sobel, E.R., McKnight, C.L., Schulein, B.J., and Wang, Z., 1992, Sedimentary record and climatic implications of recurrent deformation in the Tian Shan: Evidence from Mesozoic strata of the north Tarim, south Junggar, and Turpan basins, northwest China: Geological Society of America Bulletin, v. 104, p. 53–79.

Hendrix, M.S., Dumitru, T.A., and Graham, S.A., 1994, Late Oligocene–early Miocene unroofing in the Chinese Tian Shan: An early effect of the India-Asia collision: Geology, v. 22, p. 487–490.

Hu, A., Zhang, Z., Liu, J., Peng, J., Zhang, J., Zhao, D., Yang, S., and Zhou, W., 1986, U-Pb age and evolution of Precambrian metamorphic rocks of the middle Tianshan uplift zone, eastern Tianshan, China: Geochimica, v. 1986, p. 23–35.

Huang, D., Zhang, D., Li, J., and Huang, X., 1991, Hydrocarbon genesis of Jurassic coal measures in the Turpan basin, China: Organic Geochemistry, v. 10, p. 65–72.

Hurford, A.J., and Green, P.F., 1983, The zeta age calibration of fission-track dating: Chemical Geology, v. 41, p. 285–317.

Jiao, S.P., Zhang, Y.F., Yi, S.X., Ai, C.X., Zhao, Y.N., Wang, H.D., Xu, J.E., Hu, J.Q., and Guo, T.Y., 1988, Geological map of Qinghai-Xizang (Tibet) plateau and adjacent areas: Beijing, Geological Publishing House, scale 1:1 500 000.

Klootwijk, C.T., Gee, J.S., Peirce, J.W., Smith, G.M., and McFadden, P.L., 1992, An early India-Asia contact: Paleomagnetic constraints from Ninety East Ridge, ODP Leg 121: Geology, v. 20, p. 395–398.

Laslett, G.M., Kendall, W.S., Gleadow, A.J.W., and Duddy, I.R., 1982, Bias in the measurement of fission-track length distributions: Nuclear Tracks and Radiation Measurements, v. 6, p. 79–85.

Laslett, G.M., Green, P.F., Duddy, I.R., and Gleadow, A.J.W., 1987, Thermal annealing of fission-tracks in apatite, 2. A quantitative analysis: Chemical Geology, v. 65, p. 1–13.

Li, D., Liang, D., Jia, C., Wang, G., Wu, Q., and He, D., 1996, Hydrocarbon accumulations in the Tarim basin, China: American Association of Petroleum Geologists Bulletin, v. 80, p. 1587–1603.

Li, J., and Jiang, J., 1987, Survey of petroleum geology and the controlling factors for hydrocarbon distribution in the east part of the Junggar basin: Oil and Gas Geology, v. 8, p. 99–107.

Liou, J.G., Graham, S.A., Wang, X., Xiao, X., and Carroll, A., 1989, Proterozoic blueschist belt in western China: Best documented Precambrian blueschists in the World: Geology, v. 17, p. 1127–1131.

Ma, X., 1986, Lithospheric dynamics map of China and adjacent seas with explanatory notes: Beijing, Geological Publishing House, scale 1:4 000 000.

Matte, P., Tapponnier, P., Arnaud, N., Bourjot, L., Avouac, J.P., Vidal, P., Liu, Q., Pan Y., and Wang, Y., 1996, Tectonics of western Tibet, between the Tarim and the Indus: Earth and Planetary Science Letters, v. 142, p. 311–330.

McKnight, C.R., 1993, Structural styles and tectonic significance of Tian Shan foothill fold-thrust belts, northwest China [Ph.D. thesis]: Stanford, California, Stanford University, 207 p.

McKnight, C.R., 1994, Compressional episodes, structural styles, and shortening estimates, southern Tien Shan foreland, NW China: Geological Society of America Abstracts with Programs, v. 26, no. 7, p. 463.

Naeser, C.W., 1979, Fission track dating and geological annealing of fission-tracks, *in* Jäger, E., and Hunziker, J.C., eds., Lectures in isotope geology: New York, Springer-Verlag, p. 154–169.

Pan, Y.S., ed., 1992, Introduction to integrated scientific investigation on Karakorum and Kunlun Mountains, China: Beijing, Meterology Press, 92 p.

Patriat, P., and Achache, J., 1984, India-Eurasia collision chronology has implications for crustal shortening and driving mechanism of plates: Nature, v. 311, p. 615–621.

Roecker, S.W., Sabitova, T.M., Vinnik, L.P., Burmakov, Y.A., Golvanov, M.I., Mamatkanova, R., and Munirova, L., 1993, Three-dimensional elastic

wave velocity structure of the western and central Tien Shan: Journal of Geophysical Research, v. 98, p. 15779–15795.

Smith, A.B., 1988, Late Palaeozoic biogeography of East Asia and palaeontological constraints on plate tectonic reconstructions: Royal Society of London Philosophical Transactions, sec. A, v. 326, p. 189–227.

Sobel, E.R., 1999a, Basin analysis of the Jurassic–Lower Cretaceous southwest Tarim basin, northwest China: Geological Society of America Bulletin, v. 111, p. 709–724.

Sobel, E., 1999b, Cenozoic exhumation of the Kyrgyz Tian Shan constrained by apatite fission-track thermochronology [abs.]: Eos (Transactions, American Geophysical Union), v. 80, p. F1037.

Sobel, E.R., and Dumitru, T.A., 1997, Thrusting and exhumation around the margins of the western Tarim basin during the India-Asia collision: Journal of Geophysical Research, v. 102, p. 5043–5063.

Tapponnier, P., and Molnar, P., 1979, Active faulting and Cenozoic tectonics of the Tien Shan, Mongolia, and Baykal regions: Journal of Geophysical Research, v. 84, p. 3425–3459.

Tapponnier, P., Peltzer, G., and Armijo, R., 1986, On the mechanics of the collision between India and Asia, *in* Coward, M.P., and Ries, A. C., eds., Collision tectonics: Geological Society [London] Special Publication 19, p. 115–157.

Turcotte, D.L., and Schubert, G., 1982, Geodynamics: Applications of continuum physics to geological problems: New York, John Wiley and Sons, 450 p.

Wang, Q.M., Nishidai, T., and Coward, M.P., 1992, The Tarim basin, NW China: Formation and aspects of petroleum geology: Journal of Petroleum Geology, v. 15, p. 5–34.

Wang, Z., Wu, J., Lu, X., Zhang, J., and Liu, C., 1990, Polycyclic tectonic evolution and metallogeny of the Tianshan mountains: Beijing, Science Press, 217 p.

Watson, M.P., Hayward, A.B., Parkinson, D.N., and Zhang, Z.M., 1987, Plate tectonic history, basin development, and petroleum source rock deposition, onshore China: Marine and Petroleum Geology, v. 4, p. 205–225.

Xinjiang Bureau of Geology and Mineral Resources, 1966, Geologic map of the Kuche region: Beijing, Ministry of Geology and Mineral Resources, scale 1:200 000.

Xinjiang Bureau of Geology and Mineral Resources, 1985, Geological map of southwestern Xinjiang: Beijing, Geological Publishing House, scale 1:500 000.

Xinjiang Bureau of Geology and Mineral Resources, 1993, Regional geology of Xinjiang Uygur Autonomous Region: Beijing, Geological Publishing House, Geological Memoirs, ser. 1, 841 p.

Yin, A., Nie, S., Craig, P., Harrison, T.M., Ryerson, F.J., Xianglin, Q., and Geng, Y., 1998, Late Cenozoic tectonic evolution of the southern Chinese Tian Shan: Tectonics, v. 17, p. 1–27.

Zhang, H.N., 1989, Geochemical characteristics and resource prediction of Meso-Cenozoic source rocks in Tarim, *in* Institute of Petroleum Geology of the Ministry of Geology and Mineral Resources, ed., Petroleum resources—Prospects and evaluations, Selected papers on petroleum and natural gas geology, Volume 2: Beijing, Geological Publishing House, p. 53–76.

Zhang, X., 1981, Regional stratigraphic chart of northwest China, Branch of Xingiang Uygar Autonomous Region: Beijing, Geological Publishing House, 496 p. (in Chinese).

Manuscript Accepted by the Society June 5, 2000

Printed in the U.S.A.